JCI The Journal of Clinical Investigation

Resting innate-like B cells leverage sustained Notch2/mTORC1 signaling to achieve rapid and mitosis-independent plasma cell differentiation

Brian T. Gaudette, … , Ivan Maillard, David Allman

J Clin Invest. 2021;131(20):e151975. https://doi.org/10.1172/JCI151975.

Research Article Immunology

Graphical abstract

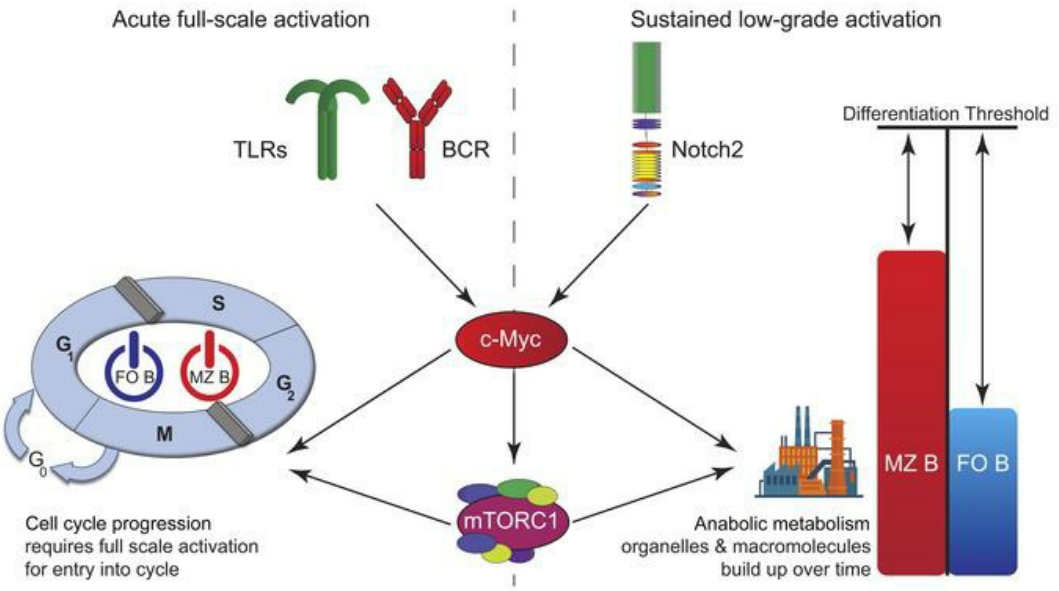

Find the latest version:

https://jci.me/151975/pdf

Resting innate-like B cells leverage sustained Notch2/mTORC1 signaling to achieve rapid and mitosis-independent plasma cell differentiation

Brian T. Gaudette,[1] Carly J. Roman,[1] Trini A. Ochoa,[1] Daniela Gómez Atria,[2] Derek D. Jones,[1] Christian W. Siebel,[3] Ivan Maillard,[2] and David Allman[1]

[1]The Department of Pathology and Laboratory Medicine and [2]The Department of Medicine, Division of Hematology/Oncology, Perelman School of Medicine at the University of Pennsylvania, Philadelphia, Pennsylvania, USA. [3]Department of Discovery Oncology, Genentech Inc., South San Francisco, California, USA.

Little is known about how cells regulate and integrate distinct biosynthetic pathways governing differentiation and cell division. For B lineage cells it is widely accepted that activated cells must complete several rounds of mitosis before yielding antibody-secreting plasma cells. However, we report that marginal zone (MZ) B cells, innate-like naive B cells known to generate plasma cells rapidly in response to blood-borne bacteria, generate functional plasma cells despite cell-cycle arrest. Further, short-term Notch2 blockade in vivo reversed division-independent differentiation potential and decreased transcript abundance for numerous mTORC1- and Myc-regulated genes. Myc loss compromised plasma cell differentiation for MZ B cells, and reciprocally induced ectopic mTORC1 signaling in follicular B cells enabled division-independent differentiation and plasma cell–affiliated gene expression. We conclude that ongoing in situ Notch2/mTORC1 signaling in MZ B cells establishes a unique cellular state that enables rapid division-independent plasma cell differentiation.

Introduction

Differentiation is often intricately tied to the cell cycle. For instance, precursors for red blood cells must proliferate to yield functional progeny (1), and embryonic stem cells are more responsive to differentiation-inducing stimuli when in the G_1 phase of the cell cycle (2, 3). Within the immune system, induced expression of transcription factors that facilitate specific helper T cell functions can also be highly cell-cycle dependent (4). It is not understood why differentiation is frequently linked to cell division or how movement to a particular phase of the cell cycle can propel cells toward a particular fate. Likewise, it is not understood how and why the role of cell division in differentiation can vary for different cell types or for cells at different developmental states within a particular lineage (5).

Early during antibody responses, activated B cells complete several rounds of mitosis before yielding antibody-secreting plasma cells. Both plasma cell differentiation and class switch recombination (CSR), 2 distinct but key processes in adaptive immunity (6), are thought to be strictly cell-cycle dependent (7, 8). Indeed, for the plasma cell fate it has been proposed that division-dependent histone modification and DNA methylation changes are required for induction of differentiation-associated gene expression (9, 10). In resting B cells, the plasma cell fate is inhibited by the transcriptional regulators Bach2 and Bcl6 (11, 12), and full plasma cell function requires decreased expression of each together with increased expression of the transcription factors Blimp1 and IRF4 (10, 13, 14). It has also been proposed that division allows dilution of these and perhaps other negative regulators (8), thereby allowing initiation of the plasma cell fate. Similarly, asymmetric division may partition positive and negative regulators into separate daughter cells, thereby permitting some offspring to yield plasma cells while others remain competent to undergo CSR and/or generate memory B cells (15). However, these ideas and observations do not incorporate other results showing that different types of B cells generate plasma cells with distinct kinetics and regulatory mechanisms.

The mature naive B cell pool consists of several subpopulations with unique roles in humoral immunity. The bulk of mature peripheral B cells are termed follicular B cells due to their propensity to recirculate through follicular structures in peripheral lymphoid organs (16). It is likely that follicular B cells dominate responses to proteinaceous antigens by generating germinal centers as well as short- and long-lived plasma cells (6). By contrast, relatively small numbers of naive B cells are actively retained in the blood-rich marginal zone (MZ) of the spleen where they dominate antibody responses to blood-borne bacteria by producing plasma cells faster and with fewer input signals compared with follicular B cells (17–20). Interestingly, resting MZ B cells possess a modestly expanded endoplasmic reticulum (ER) and increased transcript abundance for genes associated with antibody secretion and the unfolded protein response (UPR) (21, 22). How MZ B cells become poised to produce plasma cells and the full impact of this unique cellular state on host protection each remain poorly understood.

Unlike other B cells, development and maintenance of the MZ B cell pool is strictly reliant on the transmembrane receptor Notch2 (23, 24). Notch receptors have been connected to several pathways with potential relevance to early plasma cell differen-

Conflict of interest: The authors have declared that no conflict of interest exists.
Copyright: © 2021, American Society for Clinical Investigation.
Submitted: June 1, 2021; **Accepted:** August 31, 2021; **Published:** October 15, 2021.
Reference information: *J Clin Invest*. 2021;131(20):e151975.
https://doi.org/10.1172/JCI151975.

tiation. Of strong potential relevance, increased Notch signaling is associated with mTOR kinase activation in normal and malignant T cells (25–27). mTOR is a central regulator of cell growth (28), and our recent work shows that the mTOR complex known as mTORC1 is strictly required for early plasma cell genesis and that it promotes the transcription of UPR-affiliated genes in pre-plasma cells and resting MZ B cells (22, 29). A connection between mTORC1 and early plasma cell differentiation is also supported by previous work showing that mutation of *Tsc1*, a negative regulator of mTORC1 (30), allows plasma cell differentiation to initiate even in the absence of the central UPR regulator Xbp1 (31, 32). Notch also promotes transcription of the protooncogene Myc in malignant B and T cells, as well as in developing pre–T cells (33–35). Myc has a profound effect on multiple aspects of cellular function, including the cell cycle (36). Nonetheless, the impact of Notch2 activity on B cell function beyond induction and maintenance of the MZ B cell pool remains largely unknown.

We set out to study the mechanisms whereby innate-like B cells become primed to generate plasma cells. We found that MZ B cells generate Blimp1$^+$ plasma cells despite induced cell-cycle arrest, in stark contrast to follicular B cells. Furthermore, short-term blockade of in situ Notch2 signaling caused MZ B cells to acquire division-dependent plasma cell induction properties that mirrored those of normal follicular B cells. Notch2 inhibition was accompanied by rapid downregulation of Myc and mTORC1-affiliated gene expression. Sustained Myc inactivation compromised proliferation and early plasma cell induction for MZ B cells. In contrast, induced *Tsc1* mutation in resting follicular B cells fostered division-independent plasma cell differentiation potential accompanied by the increased abundance of many plasma cell and UPR-affiliated transcripts. Thus, we propose that innate-like naive B cells localized to the splenic MZ leverage ongoing Notch2/mTORC1 signaling to establish a unique cellular state that enables rapid division-independent plasma cell differentiation.

Results

Division-independent plasma cell differentiation. Our chief objective was to learn how signals received by naive B cells impact the efficiency and kinetics with which they yield plasma cells upon activation. To evaluate plasma cell induction kinetics vis a vis cell division, we first leveraged an in vitro plasma cell induction assay in which purified cell trace violet–labeled (CTV-labeled) follicular or MZ B cells are stimulated with the TLR9 agonist CpG with or without adding IL-4 and IL-5. We recently used this approach to show that CpG-stimulated MZ B cells readily generate functional plasma cells within 48 hours without cytokine supplementation, whereas CpG-stimulated follicular B cells require 72 hours and additional cytokines (22).

With this system, we compared the impact of several cell-cycle inhibitors on the capacity of follicular (CD19$^+$ AA4.1$^-$ CD23$^+$ CD21^{int}) and MZ (CD19$^+$ AA4.1$^-$ CD23^{lo} CD21^{hi}) B cells to generate plasma cells. We used the G_1 inhibitor PD0332991, the S-phase inhibitors aphidicolin or etoposide, or the G_2/M inhibitors colcemid, nocodazole, or paclitaxel. Here we gauged early plasma cell induction by measuring upregulation of Blimp1 using adult B6.Blimp1$^{+/GFP}$ reporter mice (37). As shown in Figure 1A, for follicular B cells each compound inhibited proliferation and the generation of Blimp1/GFP$^+$ cells. In sharp contrast, none of these compounds prevented the induction of Blimp1/GFP from MZ B cells, despite the expected impact on proliferation. Consequently, MZ B cell–derived Blimp1/GFP$^+$ cells that had not completed a single round of division were readily evident. Of note, we performed extensive titration experiments with each inhibitor to define optimal concentrations with minimal cell death (Supplemental Figure 1, A–C; supplemental material available online with this article; https://doi.org/10.1172/JCI151975DS1), guided by past work with primary mouse thymocytes (38). Further evidence for uncoupling of differentiation and proliferation derived from experiments where we added suboptimal concentrations of aphidicolin to stimulated follicular B cells, which caused Blimp1/GFP$^+$ cells to emerge with fewer cell divisions compared with controls (Figure 1B).

To extend these findings, we evaluated the impact of full cell-cycle inhibition on the induction of functional antibody-secreting cells using ELISpot to detect total antibody secretion. We compared the impact of PD0332991, a specific inhibitor of cyclin-dependent kinases 4/6, with a modest dose of the mTOR inhibitor rapamycin, which has been shown to cause cell-cycle arrest at the late G_1 phase of the cell cycle (39). As shown (Figure 1C and Supplemental Figure 1D), MZ B cells yielded easily detectable numbers of functional antibody-secreting cells despite division blockade, including upon mTOR inhibition, in contrast to follicular B cells. Again, the doses of PD0332991 and rapamycin used were based on earlier titration experiments (Supplemental Figure 1E).

We also used a genetic approach to inhibit cell-cycle progression. To this end, we inactivated the gene encoding cyclin dependent kinase-1 (CDK1), which is essential for B cell proliferation (40), in resting MZ B cells before inducing plasma cell differentiation in vitro. Splenocytes from mice harboring a loxP-flanked *Cdk1* allele versus WT or heterozygote littermates were incubated with increasing concentrations of Tat-Cre recombinase followed by CTV labeling and sorting of MZ B cells, before stimulation with CpG plus IL-4 and IL-5. Forty-eight hours later, we evaluated proliferation by CTV dilution and plasma cell differentiation by surface CD138 expression (flow cytometry) and antibody secretion (ELISpot). A quantity of 3 μM Tat-Cre was sufficient to constrain cell division in *Cdk1$^{fl/fl}$* cells, in contrast to lower doses, without differences in viability between WT, *Cdk1$^{+/fl}$*, and *Cdk1$^{fl/fl}$* cells (Supplemental Figure 2, A–E, and not shown). Notably, the proportion of undivided cells expressing CD138 increased substantially for *Cdk1$^{fl/fl}$* cells (Figure 2, A and B). Furthermore, ELISpot analyses of cells sorted based on division number (zero versus 1 or more) confirmed that frequencies of antibody-secreting plasma cells among undivided cells were far greater for stimulated *Cdk1$^{fl/fl}$* as compared with control *Cdk1$^{+/fl}$* MZ B cells (Figure 2C). These data further suggest that MZ B cells generate functional plasma cells independently of cell division.

To test whether MZ B cells generate plasma cells without completing mitosis in vivo, we leveraged a previously published in vivo cell surface protein labeling protocol wherein mice are inoculated with biotin and surface labeling quantified ex vivo with fluorescently labeled streptavidin (41). As cells complete mitosis, their share of biotin is divided among daughter cells, thus providing a measure of proliferation. Further, to control these experiments, the degree of biotin loss can be compared

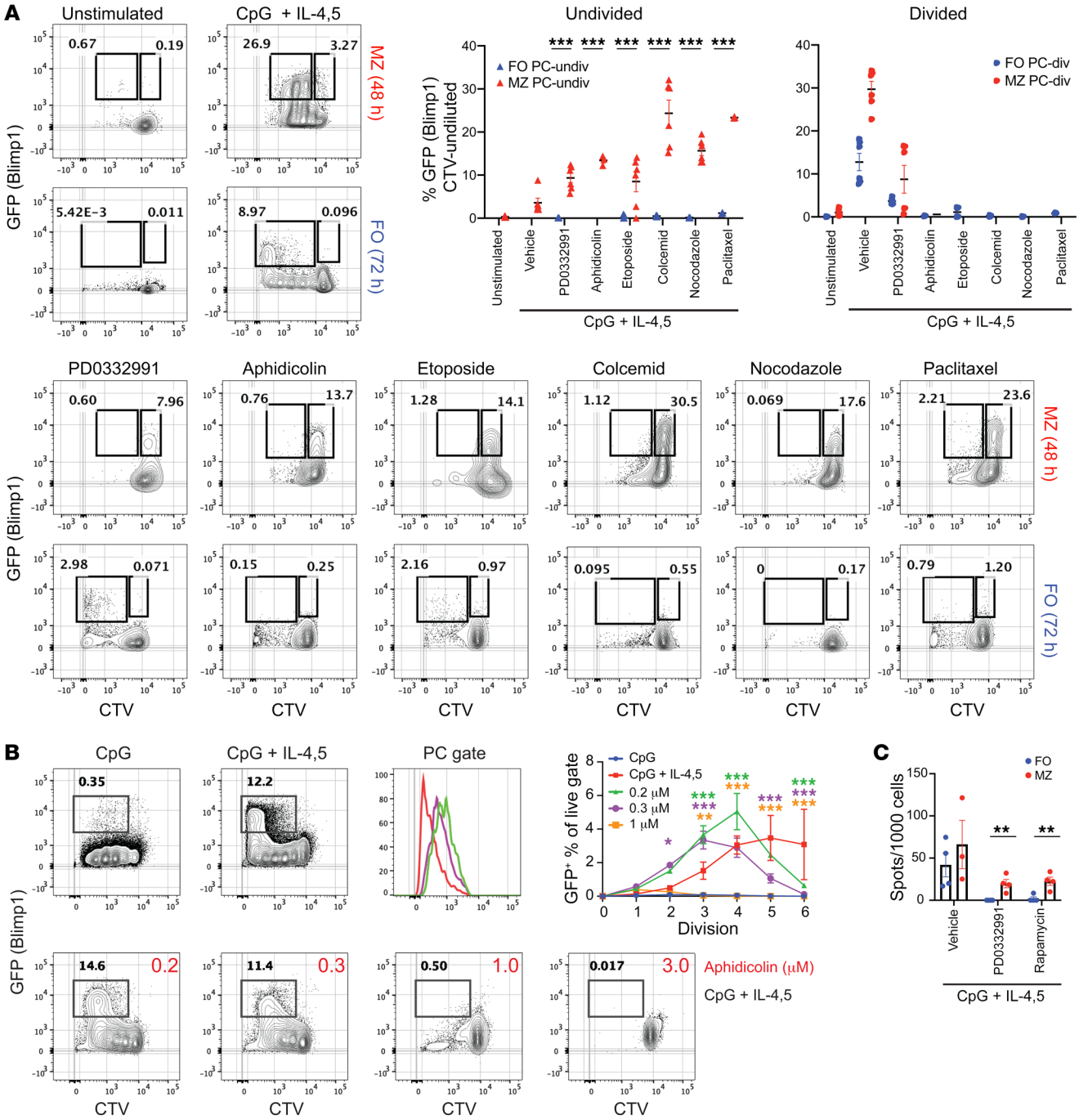

Figure 1. Marginal zone B cells generate plasma cells without dividing. (**A**) Splenic CTV-labeled MZ and follicular (FO) B cells were sort purified from B6.Blimp1$^{GFP/+}$ mice and stimulated in culture with CpG + IL-4 and IL-5 with and without the indicated cell cycle inhibitors. Resulting cells were analyzed by flow cytometry after 48 or 72 hours as indicated. Summary data are individual values, mean ± SEM. ***Adjusted $P < 0.001$, 2-way ANOVA, Sidak test for multiple comparisons between cell types. (**B**) FO B cells stimulated as in **A** with titrated concentrations of aphidicolin were evaluated at 72 hours. Histogram overlay shows CTV dilution at each aphidicolin concentration and graph shows percentage of GFP⁺ cells as a function of all viable cells at each division number. Line shows mean ± SEM. *$P < 0.05$, **$P < 0.01$, ***$P < 0.001$, compared with vehicle control using 2-way ANOVA Tukey test. (**C**) Cells prepared as in **A** were stimulated for 72 hours in culture with CpG plus IL-4 and IL-5 with or without PD0332991 or rapamycin. Graded numbers of cells from control cultures that had divided thrice, or undivided cells from cultures containing inhibitors were sorted and added to ELISpot plates. Summary data are individual values, mean ± SEM. **FDR $q < 0.01$, multiple t tests, 2-stage linear step-up procedure of Benjamini, Krieger and Yekutieli, with Q = 5%.

for populations with known degrees of steady-state proliferation such as nondividing bone marrow erythrocytes versus proliferative erythroblasts (ref. 41 and Supplemental Figure 3A). For these experiments we also exploited 2 distinctive features of MZ B cells: their unique hyper-responsiveness to lipopolysaccharide (LPS), and the capacity of anti–Notch2 antibodies to selectively deplete the MZ B cell pool after 5 to 6 days in WT mice (refs. 24, 42 and Supplemental Figure 3B).

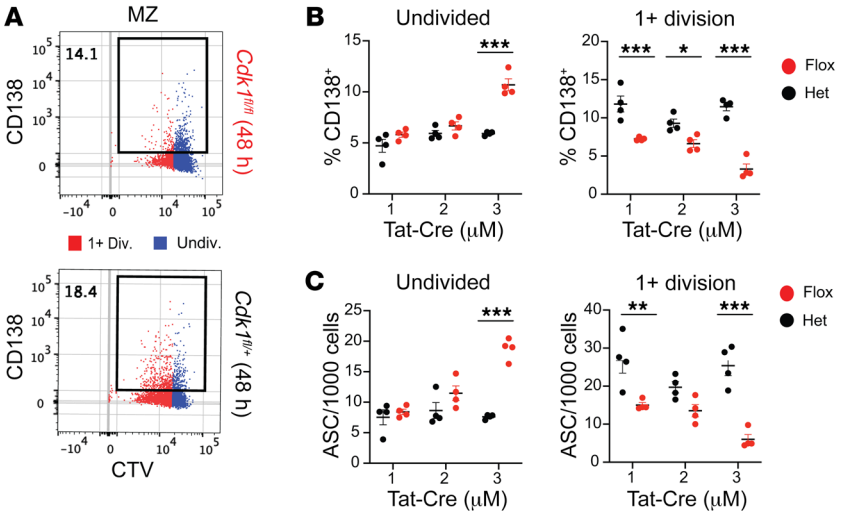

Figure 2. MZ B cells differentiate despite CDK1 deficiency. Splenocytes from *Cdk1*$^{fl/fl}$ and *Cdk1*$^{fl/+}$ littermates were treated with the indicated concentrations of Tat-Cre, then CTV-labeled and sorted. Resulting MZ B cells were cultured for 48 hours with CpG plus IL-4 and IL-5 followed by analysis by flow cytometry and ELISpot. (**A**) Overlay dot plots for CD138 surface expression pregated on undivided cells (blue) versus cells experiencing at least one division (red). (**B**) Summary data for all samples described in **A**. (**C**) Summary data showing the absolute numbers of ASC generated from undivided cells versus those that had divided one or more time. (**B** and **C**) Summary data are individual values, mean ± SEM. *Adjusted $P < 0.05$, **$P < 0.01$, ***$P < 0.001$, 2-way ANOVA, Sidak test for multiple comparisons between genotypes.

We administered NHS-biotin via a single i.v. dose 15 minutes prior to i.p. immunization of C57BL/6 adults with LPS conjugated to the hapten (4-hydroxy-3-nitrophenyl)acetyl (NP-LPS). At 36 hours after immunization, we observed small numbers of NP-binding splenic plasma cells as defined by the surface phenotype CD138$^+$ Sca1$^+$ and increased cellular volume relative to activated NP-specific CD138$^-$ splenic B cells (Supplemental Figure 3, C and D). Notably, numbers of NP-binding plasma cells were severely reduced in animals in which MZ B cells were first depleted with anti–Notch2 antibodies (Figure 3A). Further, at 36 hours after immunization the degree of biotin labeling for NP-specific plasma cells overlapped with resting follicular B cells from naive mice and was slightly higher than on erythrocytes from immunized animals (Figure 3, B and C). As expected, levels of biotin were substantially lower on bone marrow erythroblasts resolved from nondividing erythrocytes (Figure 3, B and C). By contrast, at 60 hours after immunization biotin levels for NP-specific plasma cells were reduced, indicating that all plasma cells had by then experienced cell division (Figure 3, A–C). Also, and as expected, at 60 hours, NP-specific plasma cells had increased in number, except in mice previously given anti–Notch2 antibodies, in which they remained low. The effective depletion of LPS-responsive B cells due to a previous 6 days of Notch2 blockade was further substantiated by ELISPOT and ELISA analyses of splenocytes and sera 96 hours after immunization, respectively (Figure 3, A, D, and E). Altogether, the data in Figures 1–3 indicate that MZ B cells generate plasma cells via a division-independent mechanism, in contrast to follicular B cells.

Division-independent induction of UPR genes. We evaluated gene expression in division-inhibited B cells using RNAseq. Follicular and MZ B cells harvested from B6.Blimp1$^{+/GFP}$ adults were stimulated with CpG plus IL-4/5, and the G_1 inhibitor PD0332991 or rapamycin was added. In Supplemental Figure 4 we illustrate representative data on proliferation and Blimp1/GFP expression under these conditions. Despite cell-cycle blockade, transcript abundance for numerous regulators of the acute stress response was increased in stimulated follicular and MZ B cells (Figure 4A, top). However, in the presence of PD0332991 or rapamycin, stimulated follicular B cells failed to increase transcript abundance for numerous UPR regulators related to protein secretion and plasma cell function. In stark contrast, induction of these UPR-affiliated genes was largely intact in stimulated, mitosis arrested MZ B cells (Figure 4A, bottom). Further, stimulated MZ B cells exhibited significantly enriched expression of Protein Secretion Hallmark genes when compared with unstimulated MZ B cells, despite cell-cycle inhibition (Figure 4B). Irrespective of cell-cycle inhibition, plasma cells generated from MZ B cells stimulated with CpG plus IL-4/5 were strongly enriched for the gene expression signature of mature B220$^-$ bone marrow plasma cells (Figure 4B). Relevant mitosis-independent regulators in MZ B cells included genes encoding the chaperone proteins Bip (*Hspa5*) and p58^{IPK} (*Dnajc3*), *Edem1*, which encodes the endoplasmic reticulum–associated protein degradation (ERAD) pathway regulator Edem1 (43), *Pdia6*, which encodes protein disulfide isomerase A6 (PDIA6) needed for disulfide bond formation, *Hsp90b1*, which encodes GRP94, a major immunoglobulin binding chaperone, and *Xbp1* (Figure 4, A and C). Furthermore, upon cell-cycle blockade, MZ B cells showed no difference in the upregulation of Blimp-1 (*Prdm1*) and only partial defect in downregulation of Pax5 (Figure 4C). Surprisingly, both the G1 inhibitor PD0332991 and rapamycin resulted in increased *Bach2* expression in both follicular and MZ B cells (Figure 4C). Also of note, PD0332991 but not rapamycin abrogated induction of the cell-cycle genes *Aurka*, *Cdk1,* or *Top2a* in MZ B cells (Figure 4C). Based on the data in Figures 1–4, we concluded that MZ B cells can adopt a functional plasma cell differentiation program independently of cell division.

Notch2 promotes plasma cell priming. To test the possibility that ongoing Notch2 signaling fosters division-independent plasma cell differentiation potential, we defined the impact of perturbing in situ Notch2–Notch ligand interactions on MZ B cell gene expression and plasma cell induction kinetics as a function of division number. Whereas administration of anti–Notch2 antibodies over 6 days led to the loss of MZ B cells (Supplemental Figure 3B and refs. 24, 42), with this approach numbers of MZ B cells were unchanged at 12 to 24 hours, and substantial numbers remained at 48 hours (Figure 5A). Flow cytometric analysis of MZ B cells at 12 and 48 hours after a single dose of anti–Notch2 antibodies revealed sig-

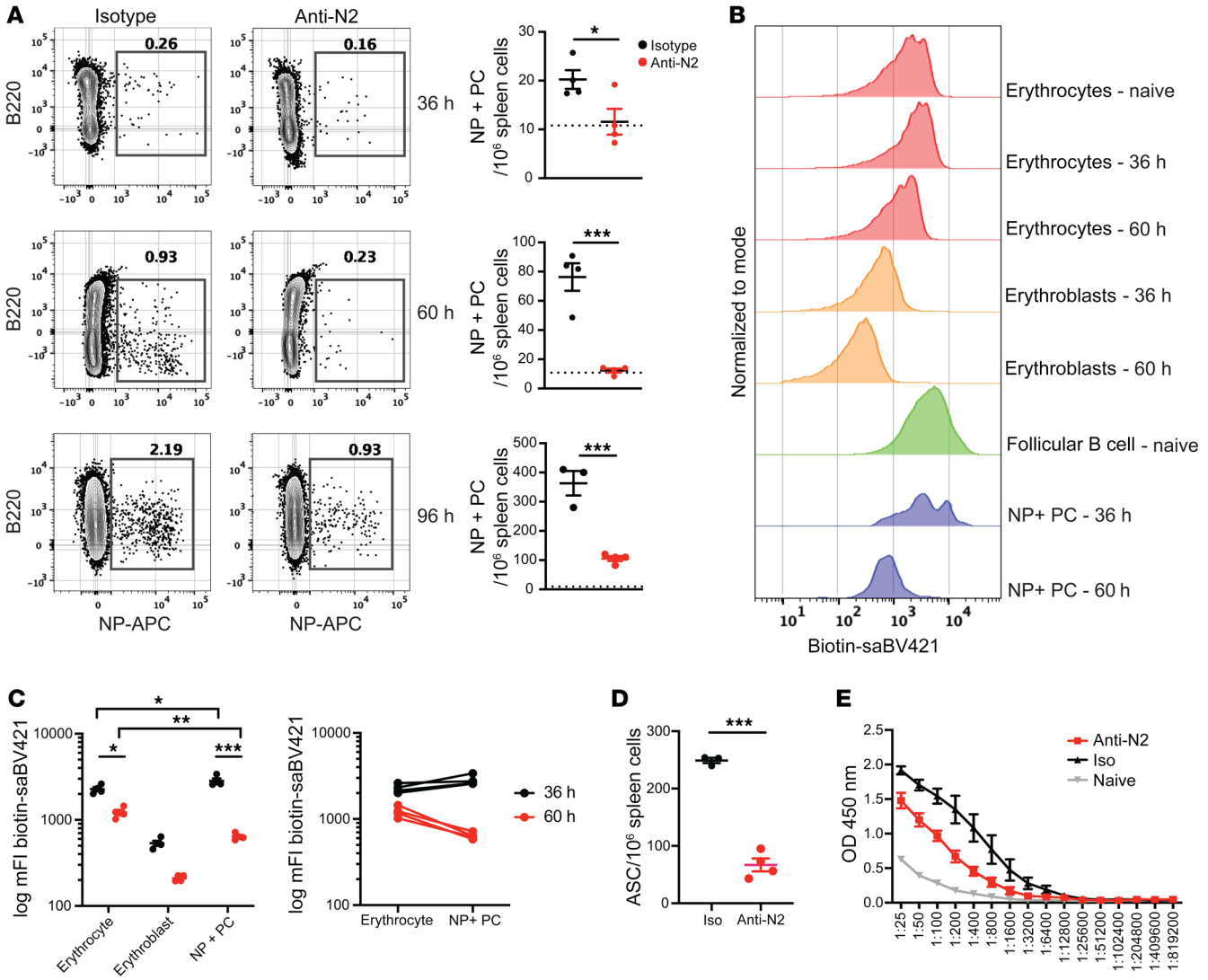

Figure 3. Rapid in vivo response to LPS without cell division. (**A**–**C**) C57BL/6 mice were depleted of MZ B cells by administering anti–Notch2 antibodies at 6 and 3 days before immunization and at the time of immunization. At 15 minutes prior to i.p. immunization with 50 μg NP-LPS, animals were inoculated i.v. with 1 mg NHS-biotin. (**A**) NP-specific plasma cells (PCs) were measured by flow cytometry (pregated on live singlet, IgD$^-$, Dump[CD4, CD8α, F4/80, Ter119]$^-$, Sca-1$^+$, CD138$^+$) at the indicated time points. Dotted line indicates background NP-binding levels in naive animals. (**B**) Histograms of indicated populations showing levels of biotin labeling by streptavidin BV421 staining. Erythrocytes (IgD$^-$, Dump[CD4, CD8α, F4/80]$^-$, Sca-1$^-$, CD138$^-$, Ter119$^+$, anucleate [by FSC/SSC]) and erythroblasts (IgD$^-$, Dump[CD4, CD8α, F4/80]$^-$, Sca-1$^-$, CD138$^-$, Ter119$^+$, nucleated [by FSC/SSC]) were gated from corresponding bone marrow from each mouse. Naive follicular B cells (live/singlet, IgD^{hi}, Dump[CD4, CD8α, F4/80, Ter119]$^-$, B220$^+$) and NP$^+$ PCs (as above) were gated from the spleens of corresponding mice. (**C**) Summary data of median fluorescence intensity of biotin labeling for indicated populations for all mice. (**D**) ELISpot assay was performed 96 hours after immunization. Indicated are the calculated numbers of ASCs per million splenocytes. (**E**) Serum ELISA for NP-specific antibody was performed on sera taken at sacrifice at 96 hours. Data are individual values, mean ± SEM. For **A** and **D**: $^*P < 0.05$, $^{**}P < 0.01$, $^{***}P < 0.001$ unpaired 2-tailed Student's *t* test. For **C**: 2-way ANOVA, Tukey post test, $^*P < 0.05$, $^{**}P < 0.01$, $^{***}P < 0.001$.

nificant and progressive downregulated expression of CD21/35 encoded by the Notch target gene *Cr2*, accompanied by a modest decrease in CD1d mean fluorescence intensity (Supplemental Figure 5A). We also observed small but significant decreases in cell size and phosphorylated S6 protein (pS6) in MZ B cells (Supplemental Figure 5, B and C). RNAseq analyses of follicular and MZ B cells at 12, 24, and 48 hours revealed changes in mRNA abundance for numerous genes in MZ B cells, with numbers of differentially expressed genes increasing over time (Figure 5B). As expected, the canonical Notch targets *Hes1*, *Dtx1*, and *Cr2* were among the genes affected at early time points (Figure 5, B and C). Importantly however, within 12 hours numerous additional transcripts were also affected. Virtually identical changes in mRNA abundance for specific loci were observed in MZ B cells after administration of antibodies that block in situ access to the relevant Notch2 ligand Delta-like1 (Dll1) (data not shown). As Dll1 ligands are expressed by nonhematopoietic stromal cells that reside close to the spleen marginal zone (44), these data suggest that MZ B cells experience continuous Dll1/Notch2-mediated signaling within the specialized MZ microenvironment. Expression of a relatively small number of genes, including *Hes1* and *Dtx1*, was also decreased by Notch2 blockade in follicular B cells, suggesting that splenic follic-

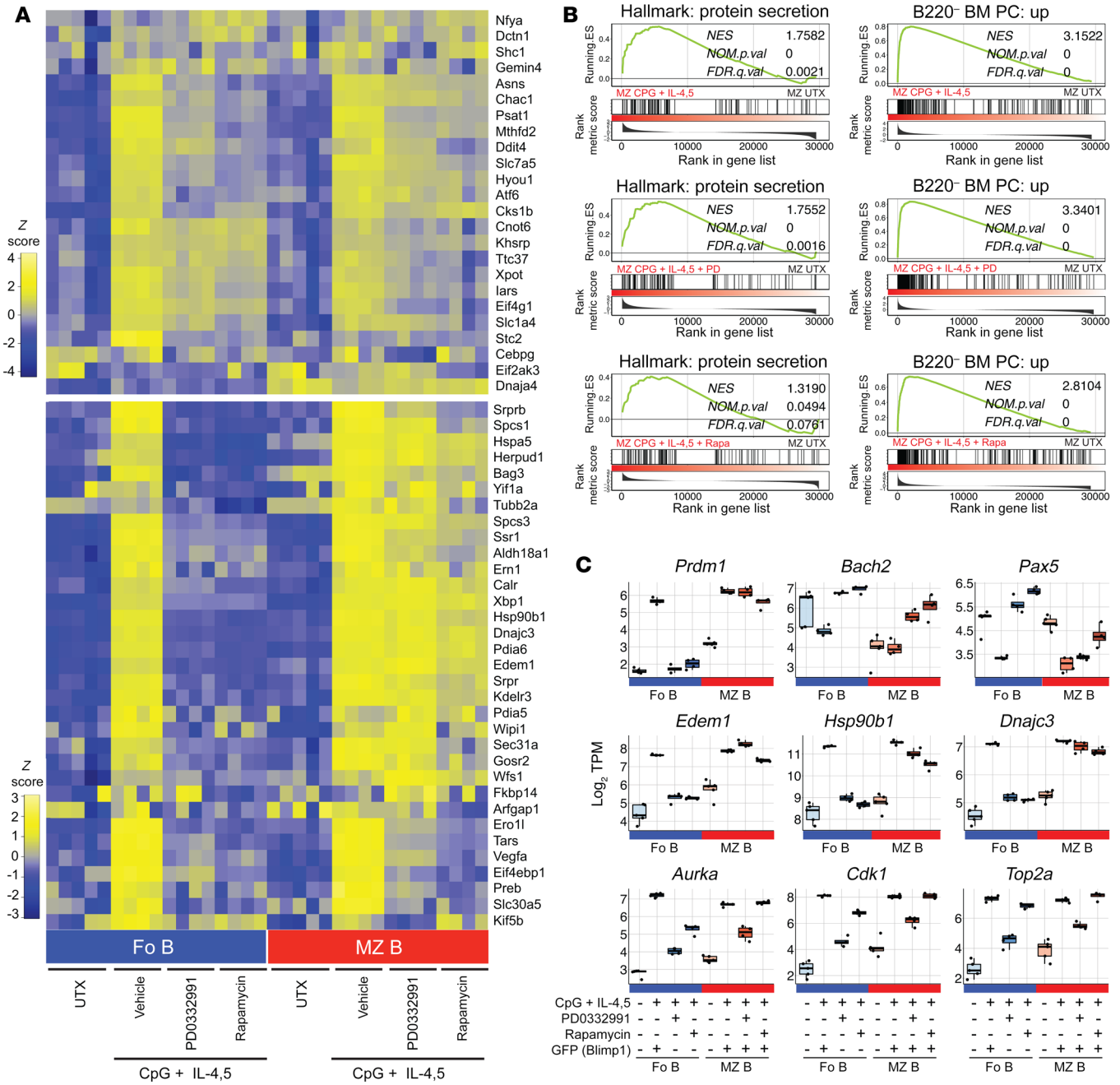

Figure 4. Induction of a plasma cell transcriptome despite cell-cycle arrest. RNAseq was performed on cells sorted as in Supplemental Figure 4. Division-inhibited cells were sorted from undiluted CTV gate. (**A**) Expression of UPR hallmark genes previously shown to be upregulated in follicular (FO) B cells treated with an activation stimulus only (CpG) (top) versus those upregulated only in follicular B cells given a plasma cell inductive stimulus (CpG plus IL-4/5) (bottom) shown as a heat map by *Z* score across each row (22). (**B**) GSEA for the Protein Secretion Hallmark gene-set (left) and B220⁻ BM plasma cell signature versus follicular B cells (right) as defined by the top 250 genes upregulated in B220⁻ BM plasma cells versus follicular B cells (22) in MZ B cells stimulated with CpG plus IL-4/5 compared with freshly isolated cells with and without cell-cycle inhibition by PD0332991 or rapamycin is shown. NES: Normalized Enrichment Score; Nom.p.val: Nominal *P* value; and FDR.q.val: FDR q value. FDR-q computed using 1000 gene-set permutations. (**C**) Log_2 TPM for the indicated genes is shown as the mean (line), 75% CI (box) and 95% CI (whisker) together with individual data points (jitter). All RNAseq data shown are prepared from 4 to 5 animal replicates.

ular B cells experience continuous but likely less intense exposure to Notch ligands as compared with MZ B cells.

Of note, compared with follicular B cells, resting MZ B cells possessed significantly higher transcript abundance for *Myc*, and within 12 hours of Notch2 blockade *Myc* mRNA abundance in MZ B cells dropped to levels observed in follicular B cells (Figure 5, B and C). Moreover, gene set enrichment analysis (GSEA) revealed decreased expression of large numbers of established Myc target genes (including ChIP-verified Myc targets in human lymphoma cells) and deregulation of numerous genes associated with mTOR

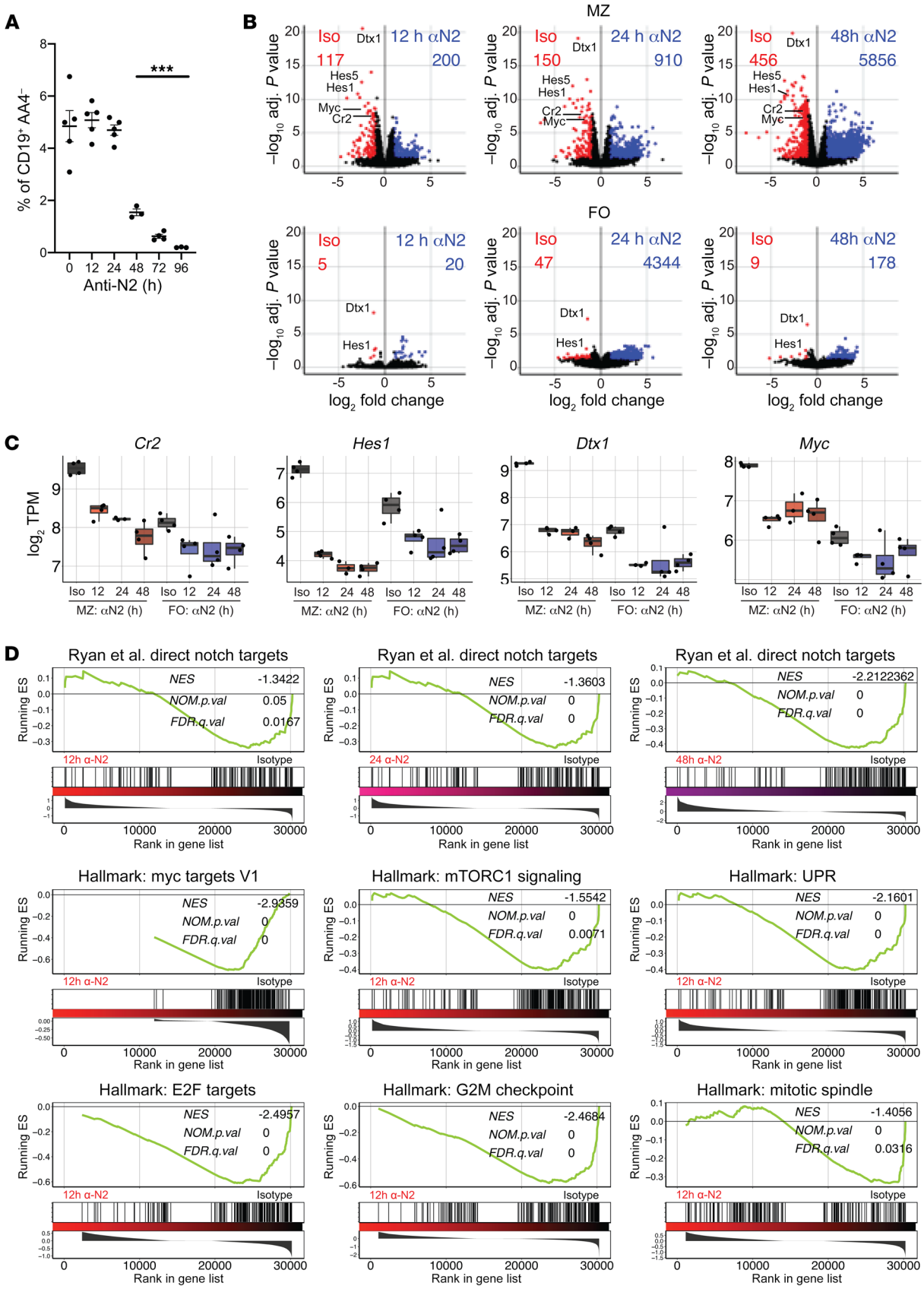
A
% of CD19+ AA4−
***
Anti-N2 (h)
B
MZ
FO
Iso
12 h αN2
24 h αN2
48h αN2
117
200
150
910
456
5856
5
20
47
4344
9
178
Dtx1
Hes5
Hes1
Myc
Cr2
−log10 adj. P value
log2 fold change
C
Cr2
Hes1
Dtx1
Myc
log2 TPM
MZ: αN2 (h)
FO: αN2 (h)
D
Ryan et al. direct notch targets
NES
NOM.p.val
FDR.q.val
-1.3422
0.05
0.0167
-1.3603
0
0
-2.2122362
0
0
12h α-N2
24 α-N2
48h α-N2
Isotype
Running ES
Rank in gene list
Hallmark: myc targets V1
-2.9359
Hallmark: mTORC1 signaling
-1.5542
0.0071
Hallmark: UPR
-2.1601
Hallmark: E2F targets
-2.4957
Hallmark: G2M checkpoint
-2.4684
Hallmark: mitotic spindle
-1.4056
0.0316

Figure 5. Sustained Notch2 signaling maintains function-related gene expression for MZ B cells. C57BL/6 mice were treated with anti–Notch2 (N2) blocking or isotype control antibodies (Iso) for up to 96 hours. Splenocytes were analyzed by flow cytometry at the indicated time points. (**A**) Shown is the relative proportion of mature splenic B cells (live, singlet $CD19^+$, $AA4.1^-$) consisting of $CD23^-$, $CD1d^+$, IgM^{hi} MZ B cells. Symbols represent data from individual mice with means indicated by horizontal lines. Individual values, mean ± SEM. ***$P < 0.001$ 1-way ANOVA, Dunnett's multiple comparison to isotype control (t = 0). (**B**–**D**) RNAseq was performed with the indicated sorted splenic B cell populations at 12, 24, and 48 hours after anti-Notch2 administration versus at 48 hours for isotype controls. (**B**) Volcano plots displaying the fold change in $\log_2$ TPM versus significance ($-\log_{10}$ adjusted *P* value, eBayes method with Benjamini-Hochberg correction) for all gene expression changes between Notch-deprived MZ (top) and follicular (FO, bottom) B cells and their respective isotype controls at the indicated time points. Genes are color-coded as follows: red: down in Notch2 blockade versus isotype control, adjusted $P < 0.05$, lfc > 1; blue: up in Notch2 blockade versus isotype control, adjusted $P < 0.05$, lfc > 1. Canonical Notch targets are indicated. (**C**) $\log_2$ TPM data for canonical Notch target gene transcripts showing the mean (bar) and 75% CI (box) and 95% CI (whisker). (**D**) GSEA for ChIP-seq verified human Notch targets at 12, 24, or 48 hours after giving anti–N2 antibodies (top, left to right) (34), as well as for Myc targets and gene sets affiliated with plasma cell function and/or the cell cycle at 48 hours. NES: Normalized Enrichment Score; Nom.p.val: Nominal *P* value; and FDR.q.val: FDR *q* value are shown. FDR-q computed using 1000 gene-set permutations. All RNAseq data are compiled from 4 animals per treatment group and time point.

signaling (Figure 5D and ref. 34). Indeed, within 12 hours, 87 of 200 known Myc targets and 42 of 200 mTORC1 signaling-associated genes were significantly dysregulated (Figure 5D and Supplemental Figure 5D), in addition to numerous genes affiliated with the UPR, E2F pathway, and others involved in G_2M checkpoint regulation or mitotic spindle formation (Figure 5D).

Next, we tested if short-term Notch2 blockade caused MZ B cells to acquire plasma cell inductive properties that mirror unmanipulated follicular B cells. Here, we again leveraged the disparate differentiation induction requirements and kinetics of freshly isolated follicular and MZ B cells as described above and illustrated in Figure 1 and our recently published work (22). Hence, here we specifically sought to determine whether Notch2 deprivation caused CpG-stimulated MZ B cells to acquire cytokine-dependent (IL-4/5–dependent) and division-dependent plasma cell induction properties. Accordingly, we sort purified MZ B cells 48 hours after i.p. administration of isotype control or anti–Notch2 antibodies. First, we evaluated plasma cell induction as a function of cell division number after stimulating all CTV-labeled cells with CpG plus IL-4/5 for 48 or 72 hours. Notably, unlike their counterparts from isotype control–treated mice, Notch2-deprived MZ B cells yielded few if any plasma cells at early division numbers (Figure 6A). Indeed, the relationship between differentiation and division number for Notch2-deprived MZ B cells mirrored normal follicular B cells (Figure 6B). Furthermore, upon Notch2 deprivation, MZ B cells acquired increased responsiveness to IL-4/5–induced amplification of CpG-stimulated plasma cell differentiation, reminiscent of follicular B cells (Figure 6C).

To examine division-dependency directly, we added PD0332991 to the in vitro cultures described in Figure 6A. For Notch2-deprived MZ B cells, functional plasma cell induction as evaluated by ELISpot was significantly compromised upon addition of PD0332991, in contrast to MZ B cells harvested from mice given isotype control antibodies (Figure 6, D and E). Importantly, we did not observe significant changes in viability for MZ B cells upon in vivo Notch2 blockade (Supplemental Figure 6). Therefore, we conclude that short-term interruption of Notch2 signaling causes MZ B cells to acquire division-dependent plasma cell induction properties that emulate those of normal follicular B cells.

The Notch2-Myc axis in plasma cell priming. Myc is required for B cell proliferation (45), and recent data suggest that subtle variations in Myc levels determine the proliferative potential of individual B and T cells (46). To induce Myc inactivation in resting B cells in vivo before assessing plasma cell induction in vitro, we fed $Myc^{fl/fl}$ CD20-TAM-Cre and control $Myc^{+/+}$ CD20-TAM-Cre adult mice with tamoxifen laced chow for 14 or 28 days, then sort-purified splenic follicular or MZ B cells and evaluated plasma cell induction in vitro. CD20-TAM-Cre mice harbor a bacterial artificial chromosome in which the CD20 locus has been modified to provide tamoxifen-induced B cell–restricted Cre induction (47). Interestingly, the frequency of MZ B cells was not decreased among mature splenic B cells, even after 28 days, suggesting that Myc is dispensable for the maintenance of MZ B cells in vivo (Supplemental Figure 7A). Nonetheless as expected, at both time points $Myc^{fl/fl}$ follicular and MZ B cells were unable to divide, $Myc^{fl/fl}$ MZ B cells exhibited reduced intracellular Myc and pS6 levels and cellular volume, and Myc-deficient follicular B cells were unable to generate $CD138^+$ cells (Figure 7, A and B and Supplemental Figure 7, B–D). Notably, these studies revealed additional evidence for uncoupling of division and differentiation. Specifically, $Myc^{fl/fl}$ cells MZ B cells yielded small numbers of $CD138^+$ cells when harvested from mice fed tamoxifen for 14 days, but not when taken from mice fed tamoxifen for 28 days (Figure 7A). Furthermore, Myc inactivation abrogated the ability of MZ B cells to produce $CD138^+$ cells upon coincubation with PD0332991 (Figure 7B). These data provide additional evidence for the uncoupling of cell division and differentiation in MZ B cells, and also suggest that Myc operates downstream of Notch2 activation to orchestrate separate biochemical pathways necessary for proliferation and differentiation.

mTORC1 promotes plasma cell priming. Given that Notch2-deprived MZ B cells possessed decreased pS6 levels and reduced transcript abundance for numerous mTORC1 hallmark genes (Figure 5D and Supplemental Figure 5C), we hypothesized that Notch2-regulated mTORC1 activity establishes a plasma cell–poised state in MZ B cells. To test this hypothesis, we asked whether follicular B cells acquire MZ-like plasma cell inductive properties upon mutation of *Tsc1*, an essential component of the mTORC1-inhibitory TSC complex (30). Because the downstream effects of Myc signaling took 4 weeks to fade completely from MZ B cells, we also fed $Tsc1^{fl/fl}$ CD20-TAM-Cre and control animals tamoxifen for 14 versus 28 days. After 14 days, we observed no changes in frequencies of follicular or MZ B cells, nor in their plasma cell induction properties, despite modest increases in pS6 levels in each cell type before stimulation (Supplemental Figure 8, A–F). Consistent with past work, at the 28-day time point frequencies of MZ B cells were decreased to roughly 50% of control mice (Supplemental Figure 8A and ref. 48). Notably, when harvested from mice given tamoxifen for 28 days, Tsc1-deficient CpG-stim-

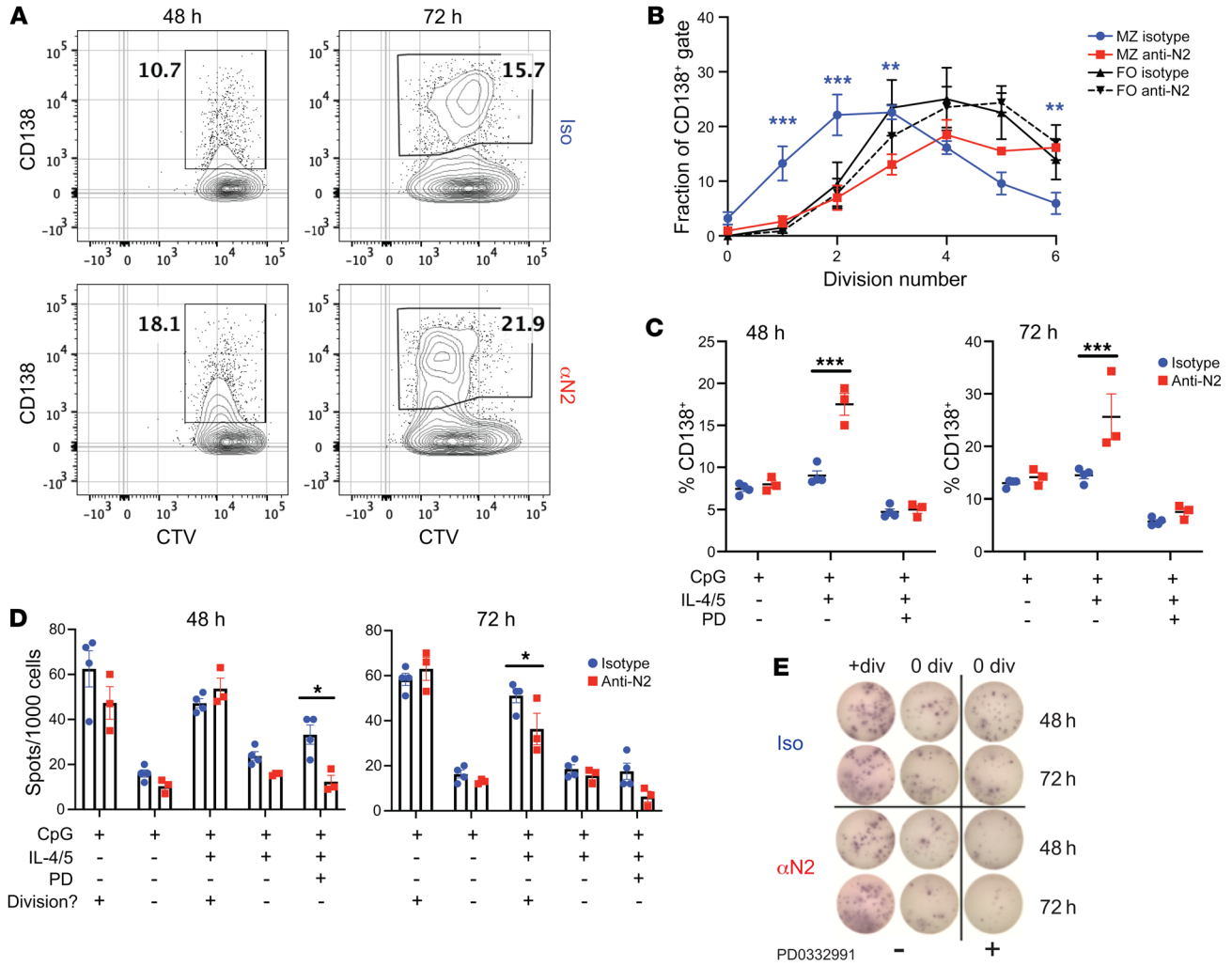

Figure 6. Sustained Notch2 signaling maintains plasma cell priming. C57BL/6 mice were treated with anti–Notch2 (αN2) or isotype control antibody for 48 hours, at which time splenocytes were harvested, CTV-labeled, and sorted MZ B cells stimulated in vitro with CpG plus IL-4/5 for 48 or 72 hours. (**A**) Cell division and CD138 expression for representative cultures at the indicated time points. (**B**) CD138 surface expression as a function of division number at 72 hours for stimulated MZ or FO B cells from the indicated treatment groups. Shown are mean and SEM for the percentage of all viable CD138$^+$ cells at the indicated division number. $^{**}P < 0.01$, $^{***}P < 0.001$. (**C**) Summary data cultures derived from 3 animals per treatment are shown as the mean and SEM for each given condition (individual values, $^{***}P < 0.001$, 2-way ANOVA, Sidak's multiple comparison test between antibody treatment groups). (**D**) Graded numbers of CD138$^+$ cells generated with the indicated stimuli were sorted into ELISpot assays to quantify functional ASCs using 3 to 4 wells/condition. PD indicates PD0332991. Shown are mean and SEM (individual values, $^*P < 0.05$, 2-way ANOVA, Sidak's multiple comparison test between antibody treatment groups). (**E**) Representative wells from **D** for undivided and cells versus cells that had experienced at least one division after stimulation with CpG plus IL-4/5 with or without PD. Data are compiled from 4 animal replicates per group and time point.

ulated follicular B cells were able to generate CD138$^+$ cells within 48 hours and without cytokine supplementation (Figure 8, A and B). Induced CD138$^+$ cells in these cultures included cells that had not completed a single round of division (Figure 8C). Importantly, ELISpot analyses confirmed that Tsc1-deficient follicular B cells produced functional plasma cells without completing a single round of division, including in the presence of PD0332991 (Figure 8, D and E). Thus, mTORC1 activation via *Tsc1* inactivation led follicular B cells to acquire division-independent plasma cell induction properties that mirrored those of WT MZ B cells.

Finally, we used RNAseq to characterize gene expression in follicular B cells after inducing *Tsc1* mutation, using twice-sorted follicular and MZ B cells derived from individual animals that were fed tamoxifen for 28 days. Focusing first on the impact on known regulators of the plasma cell fate (Figure 9A), we observed a modest increase in mRNA abundance for Blimp1 (*Prdm1*) coincident with modest decreases in *Bcl6* and *Pax5* transcripts (red versus blue and green) in follicular B cells. Furthermore, *Prdm1* mRNA abundance in *Tsc1*-mutant MZ B cells approached levels typically observed in WT plasma cells, although Pax5 transcript levels did not drop appreciably in these cells (magenta versus cyan and yellow) (Figure 9A). We did not detect changes in mRNA abundance for Bach2 (not shown), however we did note increased transcript abundance for both Atf3 and Jun to levels that approached WT MZ B cells (Figure 9A).

Notably, 192 genes were similarly differentially expressed between Tsc1-deficient versus control follicular B cells and between control MZ B cells versus follicular B cells (Supplemental Figure 9A). Gene ontology enrichment analysis of these 192 genes

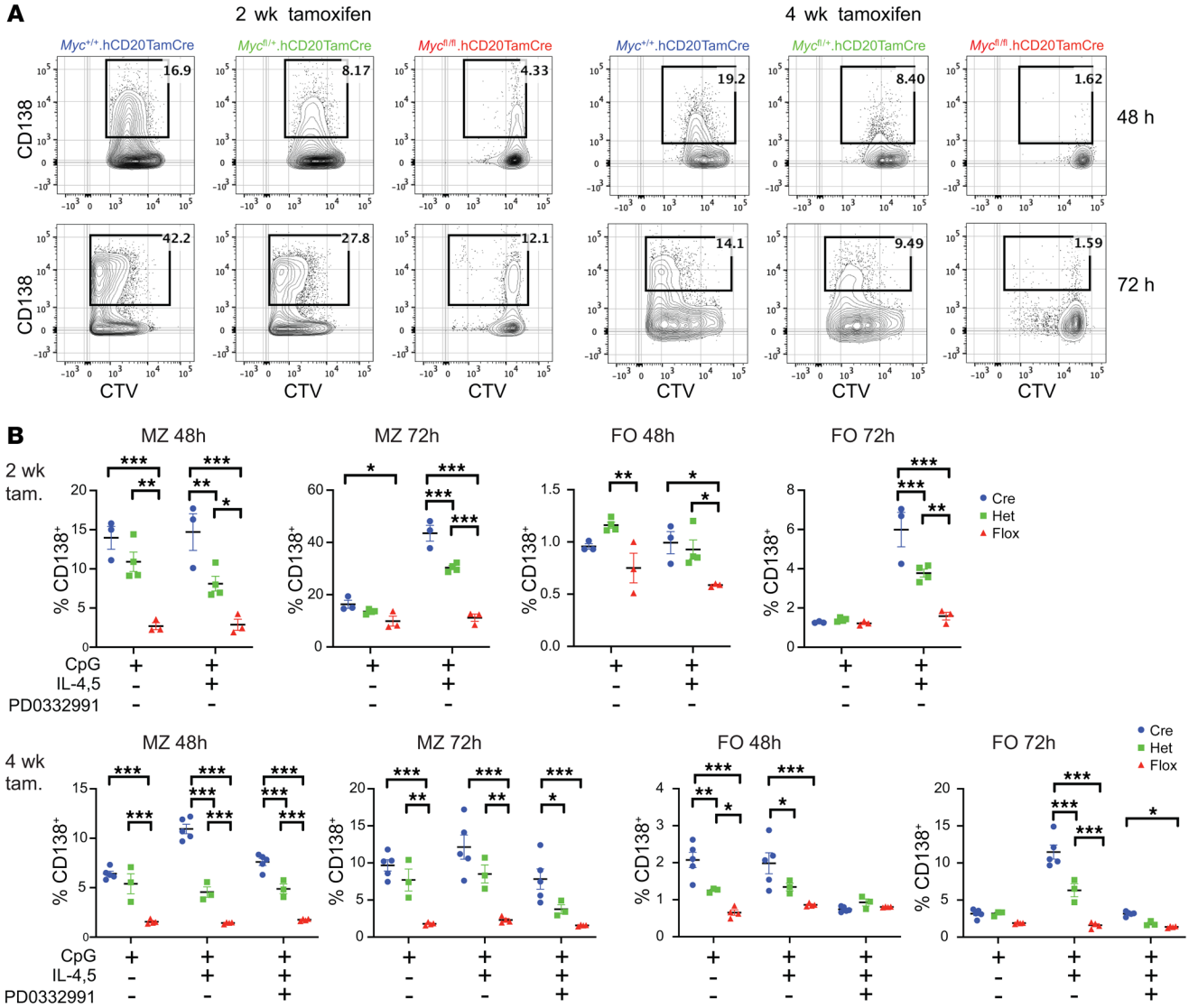

Figure 7. Myc contributes to plasma cell priming. *Myc*$^{fl/fl}$.hCD20TamCre, *Myc*$^{fl/+}$.hCD20TamCre, and *Myc*$^{+/+}$.hCD20TamCre mice were fed tamoxifen-laced chow for either 14 or 28 days. FO and MZ B cells from individual mice were CTV-labeled, sorted, and stimulated with CpG plus IL-4/5 for the indicated time periods. (**A**) Representative CD138 expression as a function of CTV dilution for MZ B cell samples. (**B**) Summary data for cultures resulting from 3 to 5 individuals per condition are shown (individual values, mean ± SEM, *$P < 0.05$, **$P < 0.01$, ***$P < 0.001$; 2-way ANOVA, Tukey's multiple comparison test between genotypes).

revealed 2 major clusters comprising over half of the enriched GO terms (32 of 61) related to lymphocyte activation and differentiation (Supplemental Figure 9B). Dimensional reduction of these differentially expressed genes by PCA illustrated how in the second principal component (29.3% of variation) *Tsc1*$^{-/-}$ follicular B cells drew even with control MZ B cells (Figure 9B). Hierarchical clustering revealed 2 clusters of genes whose expression in Tsc1-deficent follicular B cells mirrored gene expression in control MZ B cells (Figure 9C, clusters 1 and 4). We conclude that *Tsc1* ablation confers a differentiation poised molecular state in follicular B cells that mirrors WT MZ B cells.

Discussion

Our results reveal that ongoing Notch2 signaling establishes a unique biochemical state in resting innate-like MZ B cells conducive to rapid plasma cell differentiation. We further show that for MZ B cells differentiation and cell division can be easily uncoupled. Thus, while MZ B cells are likely to undergo numerous proliferative events during early plasma cell differentiation upon stimuli with exogenous antigens, the unique biochemical state of MZ B cells is such that these processes are uncoupled, in contrast to the bulk of the peripheral B cell pool. Our data also implicate the mTORC1 kinase complex downstream of Notch2 signaling as a key regulator of these processes. Thus, we propose that activation of a Notch2/mTORC1 pathway defines 2 alternative functional states for naive peripheral B cells, a Notch2/mTORC1-driven state that results in rapid division-independent plasma cell differentiation, and a Notch2/mTORC1-uninformed state defined by relatively protracted and division-dependent differentiation. Further, our results show that naive B cells are able to bypass division-driven processes

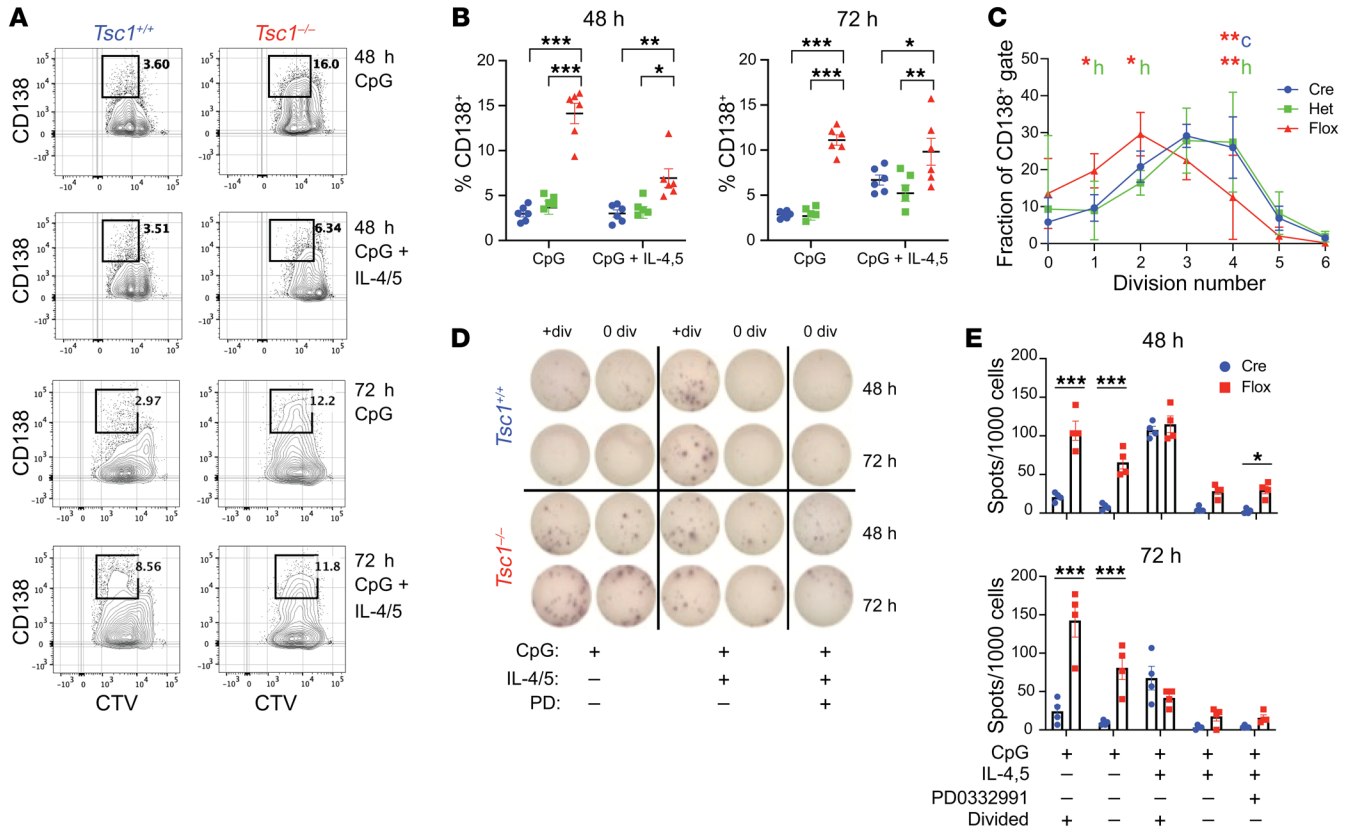

Figure 8. mTORC1 activity confers accelerated PC differentiation kinetics for follicular B cells. *Tsc1*$^{fl/fl}$.hCD20TamCre, *Tsc1*$^{fl/+}$.hCD20TamCre, and *Tsc1*$^{+/+}$.hCD20TamCre mice were fed tamoxifen in their diet for 14 or 28 days, at which point follicular B cells were CTV-labeled, sorted, then stimulated as indicated for 48 and 72 hours. (**A**) CD138 expression and CTV dilution for cultures from representative animals fed tamoxifen for 28 days are shown. (**B**) Data for cultures derived from 5 to 6 individuals per group are shown as individual points, mean and SEM. *$P < 0.05$, **$P < 0.01$, ***$P < 0.001$; 2-way ANOVA, Tukey's multiple comparison test between genotypes. (**C**) CD138 surface expression as a function of division number at 72 hours illustrating mean and SEM for the percentage of viable CD138$^+$ cells at the indicated division number. *$P < 0.05$, **$P < 0.01$; 2-way ANOVA, Tukey's multiple comparison test between color- and letter-coded genotypes. (**D**) Cultures described in **A** were sorted into ELISpot assays to quantify functional ASCs. Shown are representative wells for each treatment and time point. For undivided and postdivision cells CD138$^+$ cells were added at a dose of 300 per well. Paired wells are sorted +1 division, 0 division. (**E**) Summary of ELISpot data derived from 3 to 4 cultures per condition in **D** is shown as the individual values, mean and SEM. *$P < 0.05$, ***$P < 0.001$, 2-way ANOVA, Sidak's multiple comparison test between antibody treatment groups.

that constrain both the timing and efficiency with which the plasma cell fate is initiated as well as the magnitude of the resulting antibody response, and thus provide insights into the unique mechanisms whereby MZ B cells link innate and adaptive immunity.

Our results indicate that physical access to specific Notch ligands in the spleen determines whether peripheral B cells acquire a differentiation-poised state. Past work shows that the development and maintenance of MZ B cells requires that B cells interact with unique fibroblastic reticular cells defined by expression of the Notch ligand Delta-like-1 (DLL1) and the chemokine CCL19 (44, 49). The present study extends this information by implicating Notch2-DLL1 interactions in fostering a differentiation-poised state. Given that DLL1 is expressed by specialized nonmotile fibroblastic reticular cells (44), our observations are consistent with the concept that the Notch2/mTORC1-driven state of functional readiness in MZ B cells is controlled by in situ positional information ahead of microbial stimulation. This idea is also consistent with work suggesting that resting MZ B cells express several components of the UPR together with a modestly expanded ER (21, 22), and previous work showing that deregulated Notch signaling in developing B cells heightens MZ B cell development at the apparent expense of follicular B cells (50). Furthermore, because the MZ B cell pool develops normally in germ-free mice (51), it is likely that priming for plasma cell differentiation occurs without overt stimulation by local or systemic signals associated with infection or the microbiota. The latter conclusion is consistent with our additional data showing that plasma cell induction kinetics and genome-wide gene expression is unchanged when MZ B cells are harvested from germ-free mice (not shown). Thus, while BCR specificity can select developing B cells for colonization of the MZ B cell pool (52), such results likely reflect positive selection events mediated by BCR signals generated by low-affinity interactions with poorly defined self-ligands (53, 54).

Our data also reveal unique regulatory functions for mTORC1 in resting and activated B cells. Interestingly, mTORC1 activation is suppressed as transitional B cells mature into follicular B cells (55). Thus, whereas decreased mTORC1 activity in resting follicular B cells is key for their development and for achieving metabolic quiescence, the capacity of Tsc1 mutation to cause accelerated differentiation together with increased transcript abundance

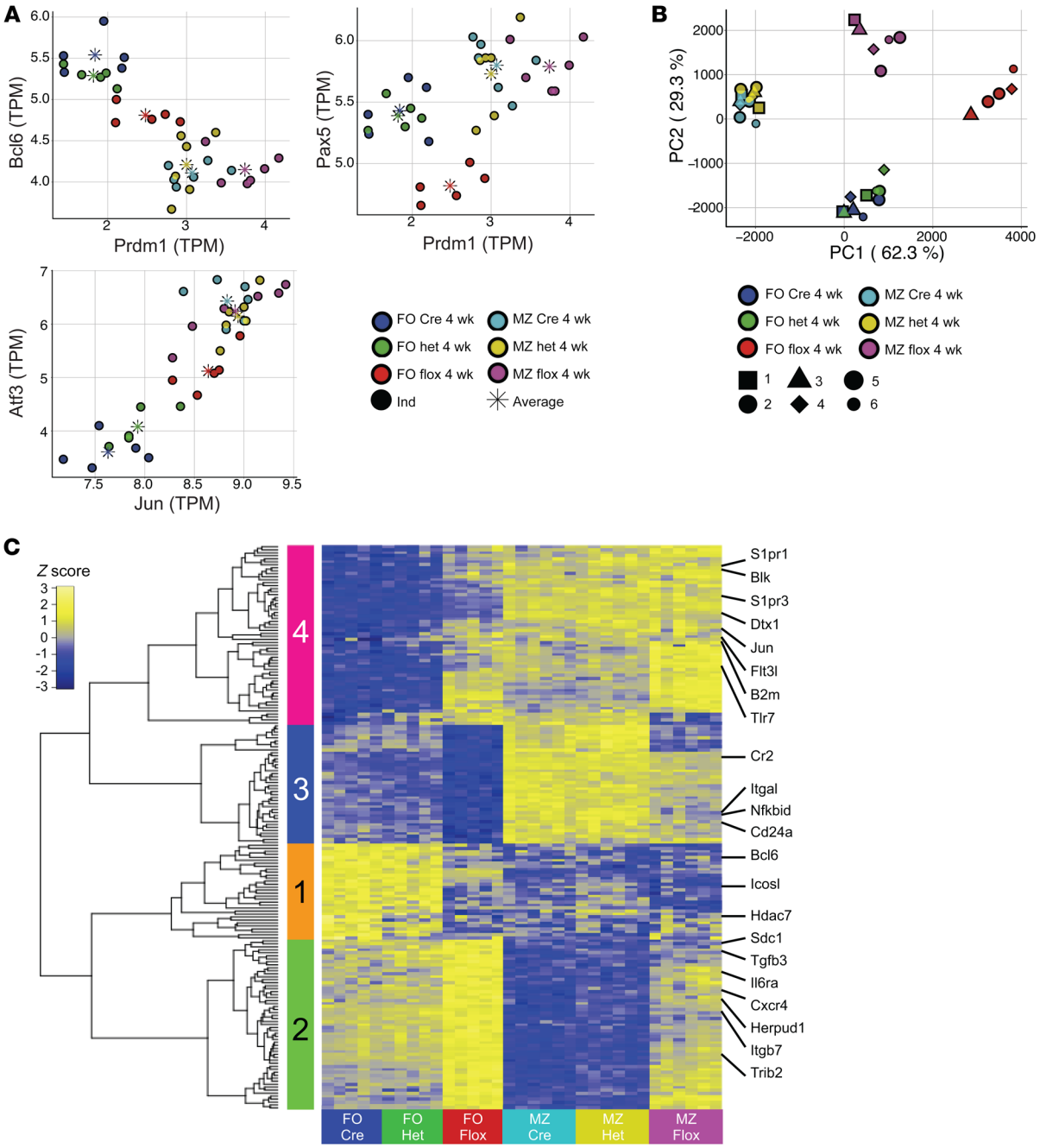

Figure 9. Increased mTORC1 activity in follicular B cells primes plasma cell gene expression. (**A**–**C**) RNAseq was performed on cDNA prepared from sorted splenic FO and MZ B cells. (**A**) A series of 2-gene comparisons of $\log_2$ TPM expression are shown for follicular and MZ B cells from each genotype after 4 weeks of tamoxifen exposure. The average for each group is indicated by an asterisk. (**B**) Dimensional reduction of 192 genes differentially expressed between *Tsc1*$^{fl/fl}$ versus Cre control follicular and MZ B cells with adjusted $P < 0.01$ is shown depicting first 2 principal components among the indicated 6 groups. (**C**) Expression of genes described in **B** is shown as *Z* scores across each row. Genes are hierarchically clustered by Pearson correlation.

for certain plasma cell–affiliated genes (Figures 8 and 9) suggests that suppression of mTORC1 function is also important for constraining plasma cell genesis. This idea is also consistent with the increased basal levels of mTORC1 activity observed in resting differentiation-poised MZ B cells and the connection of mTORC1 function to the expression of UPR-affiliated genes (Supplemental Figure 5C and ref. 22). Furthermore, the connection between mTORC1 and mRNA abundance for UPR and plasma cell–associated genes raises the possibility that mTORC1 promotes certain aspects of differentiation by amplifying the transcription of cell type– and stage-specific genes. While further work is needed, it is highly likely that the impact of mTORC1 on transcript abundance for such genes is both indirect and largely if not entirely separate from its role in proliferation.

Emerging data indicate that subpopulations of memory B cells in mice and people can adopt unique biochemical states that allow

for exceptionally rapid plasma cell differentiation (56–58). Thus, with this idea in mind we speculate that mTORC1 activity is elevated in other differentiation-poised B cells, including for certain subsets of memory B cells. Given that many memory B cells are thought to recirculate routinely between the blood and peripheral lymphoid tissues, we envision that plasma cell priming in memory B cells occurs without overt input from Notch receptor-ligand interactions. However, in the mouse, memory B cells consist of numerous functionally distinct subsets that include spleen- and lung-resident cells (57, 59). Similarly, the human spleen and peripheral blood each contain large numbers of IgM^+ $CD27^+$ B cells with characteristics of both MZ and memory B cells (60) that play important roles in humoral responses against encapsulated bacteria (61) and are responsive to Notch ligands (62). Hence it is tempting to propose that the Notch2-mTORC1 axis also establishes division-independent plasma cell differentiation in human MZ-like IgM memory B cells.

mTORC1 may also promote rapid differentiation for other naive B cells. Indeed, it has been proposed that B1 B cells spontaneously secrete IgM antibodies without canonical changes in gene expression associated with plasma cell differentiation and apparently without cell division (63). However, these results and this general idea have been challenged (64), and the need for mitosis in plasma cell function of B1 B cells has not to our knowledge been tested directly. Therefore, it may prove useful to examine whether mTORC1 drives plasma cell priming and uncoupling from cell division for B1 B cells. Importantly, however, B1 and MZ B cells differ in many relevant ways, including the capacity of B1 B cells to develop despite Notch2 mutation (23). Finally, we speculate that unique aspects of a conserved NOTCH2-regulated program can be hijacked during malignant transformation in subsets of human mature B cell lymphomas, such as marginal zone lymphomas, which are characterized by recurrent activating oncogenic *NOTCH2* gene mutations that preserve the ligand dependence of NOTCH2 activation (34, 65, 66).

The regulation of effector cell differentiation through positional access to specific Notch ligands may not be unique to B cells. Emerging evidence suggests that T cell differentiation and function can be modified due to interactions between Notch receptors on T cells and Notch ligand–bearing fibroblastic reticular cells. For instance, inactivation of *Dll4* in Ccl19-Cre^+ lymph node fibroblasts reduces follicular helper T cell numbers (44), and the activation of donor allo-reactive T cells in models of graft-versus-host disease is also inhibited upon inactivation of Notch ligand expression on Ccl19-Cre^+ fibroblasts in secondary lymphoid organs (67). Therefore, it is tempting to propose that the many outcomes of Notch–Notch ligand interactions in multicellular organisms have evolved to include the induction of gene expression programs needed for rapid adaptation to changes in local microenvironments. Within the immune system, this would therefore include the amplification of unique effector cell differentiation pathways needed for the rapid protection against acute life-threatening infection.

The role of cell division in differentiation often varies with the functional demands on precursor cells and their products. Our results suggest that MZ B cells leverage ongoing albeit relatively restrained c-Myc and mTORC1 activity, each propagated by Notch2 signaling, to sidestep division-regulated differentiation, thereby allowing rapid induction of humoral responses. Interestingly, by varying the time for inducing Myc mutation (Figure 7), we found that proliferative potential was lost faster than differentiation potential. Therefore, we speculate that B cells require greater concentrations of Myc for cell division than for initiating plasma cell differentiation. Thus, while it is abundantly clear that Myc is required to initiate and sustain germinal center B cell responses (68), it is likely that Myc also regulates numerous other aspects of B cell differentiation. Interestingly, Heinzel et al. proposed that slight increases in intracellular Myc levels in resting naive B and T cells prolongs the length of time with which activated cells can engage in mitosis (46). Therefore, given that resting MZ B cells possess higher Myc levels compared with follicular B cells, we propose that an additional outcome of the Notch2/c-Myc/mTORC1 signaling axis is to increase clonal burst size for stimulated MZ B cells and the plasmablasts they produce, thereby increasing antibody titers.

Past studies focused on other cell types suggest that mitotic cells employ unique regulatory processes to maintain cell type–specific gene expression despite the numerous changes in nuclear architecture and function inherent in proliferation. During mitosis, the nuclear envelope undergoes disassembly and reassembly, histone biogenesis and chromatin landscapes change, DNA-binding regulatory proteins become unbound, and transcription is largely silenced (69, 70). Therefore, cell type–specific chromatin landscapes and gene expression patterns must be reestablished in postproliferative daughter cells, raising the possibility that differentiation-inducing signals disrupt or override these processes. Determining whether these ideas apply to follicular B cells will require further study. Among precursors for red blood cells, the GATA1 transcription factor remains bound to mitotic chromatin in order to orchestrate the reestablishment of chromatin landscapes needed for erythroid differentiation (71). We note that an analogous factor that reestablishes cell type–pecific gene expression in postmitotic B lineage cells has not been identified. However, recent data suggest that gene expression changes in LPS-stimulated B cells are impacted by 2 discrete phases of chromatin reorganization, first before initial exit from G_1, and second coincident with plasma cell differentiation (72). Based on these results, we suggest that Notch2 signaling causes MZ B cells to acquire epigenetic modifications that are key for fostering rapid differentiation potential. Elucidation of the mechanisms whereby postproliferative B cells maintain or modify cellular identity may shed light on numerous facets of B cell differentiation, including strategies to manipulate plasma cell numbers and per cell rates of antibody synthesis.

Methods

Mice. C57BL/6 (C57BL/6J), $Cdk1^{fl}$ ($Cdk1^{L}$, $Cdk1^{tm1Eddy}$/J; ref. 73) and $Tsc1^{fl}$ ($Tsc1^{C}$, $Tsc1^{tm1Djk}$/J; ref. 74) mice were procured from Jackson Laboratories. hCD20.Tam-Cre mice (47) were provided by Mark Shlomchik (University of Pittsburgh, Pittsburgh, Pennsylvania, USA), B6.$Blimp1^{+/GFP}$ ($Prdm1^{+/GFP}$; ref. 37) mice by Stephen Nutt (Walter and Eliza Hall Institute of Medical Research, Parkville, Victoria, Australia), and $Myc^{fl/+}$ (45) mice by Doug Green (St. Jude's Children's Research Hospital, Memphis, Tennessee, USA). Tamoxifen was administered orally in tamoxifen citrate-supplemented (0.4 g/kg) mouse diet cal-

ibrated to deliver approximately 40 mg/kg body weight per day per mouse (Tekaid/Envigo TD.130859). Animals were placed on a 5-days-on, 2-days-off regimen to maintain body weight and reduce toxicity for up to 4 rounds (28 days) of treatment. In vivo Notch2 blockade was performed by i.p. administration (5 mg/kg) of a humanized IgG1 antibody specific for the Notch2 negative regulatory region (anti-NRR2), as previously described (42). Control mice received an irrelevant hIgG1 antibody specific for herpes simplex virus glycoprotein D (75).

In vivo biotin labeling. NHS-biotin (EZ-Link Sulfo-NHS-LC-LC-biotin, Thermo Scientific, catalog 21338) was prepared at 5 mg/mL in sterile PBS and administered i.v. at 200 μL or 1 mg per mouse 15 minutes prior to immunization. Visualization of biotin labeling was by staining with streptavidin BV421 (BioLegend, catalog 405225) after surface marker stain and before live/dead stain with 7AAD.

Cell preparation. Spleen cells were obtained by mechanical disruption of the spleen between 2 frosted glass slides in FACS buffer (PBS, 0.1% BSA, 1 mM EDTA) followed by filtration through 0.66 μm nitex mesh and red blood cell lysis with ACK lysis buffer.

Cell culture and stimulation. Splenocytes from 10-week-old mice were Celltrace Violet–labeled according to the manufacturer's protocol and sorted into complete growth media (RPMI, 10%FBS, HEPES, Penn/Strep, NEAA, Na-Pyruvate, 2-ME). Cells were plated at 1×10^6 cells/mL in 96-well culture plates at 200 μL/well. Cultures were supplemented as indicated with CpG DNA (0.1 μM), IL-4 (100 ng/mL), IL-5 (100 ng/mL), and rapamycin (2 nM). Cultures were incubated at 37°C, 5% CO_2 for the indicated times.

Tat-Cre treatment. Splenocytes were washed in serum free media (SFM) (RPMI, HEPES, Penn/Strep, NEAA, Na-Pyruvate, 2-ME) and resuspended in 1 mL 1, 2, or 3 μM Tat-Cre in SFM and incubated at 37°C for 30 minutes. An equal volume of 2× CTV in SFM was then added and the cells were incubated an additional 15 minutes at 37°C. The entire reaction was then quenched with 10 volumes of complete growth media (SFM + 10% FBS) and incubated for 10 minutes at 37°C. Resulting cells were then stained for FACS sorting.

Flow cytometry and sorting. Following RBC lysis, cells were stained with Zombie-Aqua Fixable Viability kit (BioLegend) according to the manufacturer's protocol and then stained with a cocktail of appropriate antibodies at optimized concentrations for 30 minutes on ice. Flow cytometry was performed using Becton Dickinson LSRII and LSR Fortessa analyzers and cell sorting with BD FACS Aria cell sorters. Data analysis was performed using Flowjo 10.6.x software. Steady-state cell populations were twice-sorted by the following gating strategies as described (16, 76): follicular B: size, singlet, live, $CD19^+$, $AA4.1^-$, $CD23^+$/$CD21/35^{mid}$; MZ B: size, singlet, live, $CD19^+$ $AA4.1^-$, $CD23^-$, $CD21/35^{hi}$.

Intracellular staining. Intracellular pS6 staining was performed using BD Cytofix and BD Phosphlow Perm Buffer III 2-step protocol. Intracellular Myc expression was analyzed using the Thermo Fisher Foxp3 Transcription Factor Staining Buffer Kit using the manufacturer's 1-step intranuclear, 96-well plate protocol.

Antibodies. CD23 (B3B4)-PE and –BV421, TCRβ (H57-597)-PE, Ter-119-PE and CD138 (281-2)-PE were purchased from BD Biosciences. IgD (11-26.2a)-APC-Cy7, CD4 (GK1.5)-PE-Cy7, Ter-119-PE-Cy7, F4-80 (BM8)-PE-Cy7, B220 (RA3-6B2)-BV421, CD1d (1B1)-PE, (1B1)-BV605, and CD138 (281-2)-BV605 were purchased from BioLegend. Myc (c-Myc, D84C12)-PE and pS6(S235/236) (D57.2.2E)-PE-Cy7 were purchased from Cell Signaling Technology. AA4.1-APC, CD21/35 (8D9)-PE-Cy7, IgM (11/41)-PerCP-ef710, and CD8α (53-6.7)-PE and –PE-Cy7 were purchased from eBioscience (Thermo Fisher Scientific). CD19 (6D5)-APC-Cy5.5 and F4-80 (BM8)-PE were purchased from Invitrogen. B220 (RA3-6B2)-APC was purchased from Tonbo Biosciences.

RNA sequencing. Cell populations were sorted directly into Trizol with 0.5% 2-ME and held at –80°C until RNA preparation. RNA was prepared by published Trizol RNA-extraction protocol (Thermo Fisher Scientific). RNA was coprecipitated using glycogen as a carrier. RNA was quantified using Qubit RNA high sensitivity fluorometric assay. cDNA was prepared using Takara Clonetech SMART-Seq HT Kit according to protocol using 500 to 1000 ng RNA as input. cDNA was quantified and qualified using high-sensitivity DNA assay on an Agilent 4200 Tapestation. RNAseq libraries were constructed using the Illumina Nextera XT kit with 150 ng cDNA input. Libraries were quality controlled and quantified by Tapestation and pooled at equal molar ratio prior to sequencing on Illumina Nextseq500 (75 bp SE v2) machines.

Pseudoalignment and gene expression. Transcript abundance was computed by pseudoalignment with Kallisto (77). Transcript per million (TPM) values were normalized and fitted to a linear model by empirical Bayes method with the Voom and Limma R packages (78, 79) and differential gene expression was defined as a Benjamini-Hochberg corrected *P* value of less than 0.05 and fold change greater than 2 unless otherwise noted.

Gene ontology cluster enrichment. GO analysis was performed using the DAVID Bioinformatics Resources 6.8 (NIAID, NIH) as well as ClueGO and Cytoscape using enrichment score calculation from Bonferroni step-down adjusted *P* values less than 0.05 to define enriched terms and clusters of terms, choosing the term with highest number of represented genes as founder term for each cluster. Nondescriptive or overly general terms were disregarded in favor of the term with the next highest number of genes represented (80–82).

Gene-set enrichment analysis. GSEA was performed using the Broad institute GSEA java tool with both curated gene sets and our described investigator-defined gene sets (83, 84).

ELISpot assay. ELISpot assay plates (Millipore MSIPN4W50) were coated with capture goat anti Ig-heavy/Ig-light antibody (Southern Biotech 1010-01) at 10 μg/mL and blocked with complete growth media (RPMI, 10%FBS, HEPES, Penn/Strep, NEAA, Na-Pyruvate, 2-ME). Cells were FACS sorted directly into complete growth media at indicated cell number or at 10^5 cells/well and serially diluted and incubated overnight. Biotinylated goat anti IgKappa plus IgLambda (Southern Biotech 1050-08, 1060-08) capture antibody was used at 0.1 μg/mL. Streptavidin alkaline phosphatase was used at 1:10,000 final dilution. Spots were developed using BCIP/NBT liquid substrate and 1M sodium phosphate stop solution. Image capture, counting, and quality control were performed using the CTL Immunospot Analyzer and software (Cellular Technologies Limited).

Statistics. Statistical analyses for all flow cytometric and ELISpot-based analyses were performed using GraphPad Prism 9. Students *t* tests were used for pairwise comparisons and 1- and 2-way ANOVA were used for multicolumn and multilevel comparisons, respectively. Posttests for multiple comparisons were chosen based on highest statistical power for each experiment based on the comparisons being made. RNAseq data analyses were performed within the R statistical environment, including the limma package where differential expression was defined by fitting a linear model and testing by the eBayes method with Benjamini-Hochberg correction for multiple compari-

sons. Unless noted, differential expression was defined by adjusted *P* less than .01 and a $\log_2$ fold change of at least 1. GSEA was performed with GSEA 4.1 using at least 1000 gene-set permutations to generate FDR *q* values. Geno-ontology analysis was performed with the ClueGO 2.2.5 plugin and Cytoscape 3.4.0 using a Bonferroni's step-down adjusted *P* value cutoff of 0.05 for enriched pathways.

Study approval. All animal procedures were approved by the University of Pennsylvania Office of Regulatory Affairs.

Data availability. RNAseq data are available in the NCBI Gene Expression Omnibus (GEO) under the following accession numbers: GSE180174 (study superseries); GSE180170: Cell-cycle inhibition PC induction; GSE180172: Notch Blockade MZ and follicular B cells; GSE180173: Tsc1-deficient MZ and follicular B cells.

Author contributions

BTG, DA, and IM designed experiments and wrote the manuscript. BTG performed experiments and all bioinformatics analyses. CJR, TAO, DDJ, and DGA performed experiments. CWS generated critical reagents.

Acknowledgments

We gratefully thank David Hildeman, Avinash Bhandoola, and Ranjan Sen for helpful discussions and Mark Shlomchik and Doug Green for generously providing CD20-TAM-Cre and Myc$^{+/fl}$ mice, respectively. We also thank the University of Pennsylvania Flow Cytometry and Cell Sorting facility. This work was supported by NIH grants AI139123 and AI154932 (to DA), AI091627 (to IM), AI139123S (to TAO), and training grant T32CA009140 (to DDJ and BTG).

Address correspondence to: David Allman, The Department of Pathology and Laboratory Medicine, Perelman School of Medicine at the University of Pennsylvania, Philadelphia, Pennsylvania 19104-6082, USA. Email: dallman@pennmedicine.upenn.edu.

1. Pop R, et al. A key commitment step in erythropoiesis is synchronized with the cell cycle clock through mutual inhibition between PU.1 and S-phase progression. *PLoS Biol*. 2010;8(9):e1000484.
2. Pauklin S, Vallier L. The cell-cycle state of stem cells determines cell fate propensity. *Cell*. 2013;155(1):135–147.
3. Sela Y, et al. Human embryonic stem cells exhibit increased propensity to differentiate during the G1 phase prior to phosphorylation of retinoblastoma protein. *Stem Cells*. 2012;30(6):1097–1108.
4. Mullen AC, et al. Cell cycle controlling the silencing and functioning of mammalian activators. *Curr Biol*. 2001;11(21):1695–1699.
5. Dalton S. G1 compartmentalization and cell fate coordination. *Cell*. 2013;155(1):13–14.
6. Goodnow CC, et al. Control systems and decision making for antibody production. *Nat Immunol*. 2010;11(8):681–688.
7. Hodgkin PD, et al. B cell differentiation and isotype switching is related to division cycle number. *J Exp Med*. 1996;184(1):277–281.
8. Nutt SL, et al. The genetic network controlling plasma cell differentiation. *Semin Immunol*. 2011;23(5):341–349.
9. Barwick BG, et al. Plasma cell differentiation is coupled to division-dependent DNA hypomethylation and gene regulation. *Nat Immunol*. 2016;17(10):1216–1225.
10. Scharer CD, et al. Antibody-secreting cell destiny emerges during the initial stages of B-cell activation. *Nat Commun*. 2020;11(1):3989.
11. Muto A, et al. Bach2 represses plasma cell gene regulatory network in B cells to promote antibody class switch. *EMBO J*. 2010;29(23):4048–4061.
12. Shaffer AL, et al. BCL-6 represses genes that function in lymphocyte differentiation, inflammation, and cell cycle control. *Immunity*. 2000;13(2):199–212.
13. Shaffer AL, et al. Blimp-1 orchestrates plasma cell differentiation by extinguishing the mature B cell gene expression program. *Immunity*. 2002;17(1):51–62.
14. Sciammas R, et al. Graded expression of interferon regulatory factor-4 coordinates isotype switching with plasma cell differentiation. *Immunity*. 2006;25(2):225–236.
15. Lin WH, et al. Asymmetric PI3K signaling driving developmental and regenerative cell fate bifurcation. *Cell Rep*. 2015;13(10):2203–2218.
16. Allman D, Pillai S. Peripheral B cell subsets. *Curr Opin Immunol*. 2008;20(2):149–157.
17. Oliver AM, et al. Marginal zone B cells exhibit unique activation, proliferative and immunoglobulin secretory responses. *Eur J Immunol*. 1997;27(9):2366–2374.
18. Lu TT, Cyster JG. Integrin-mediated long-term B cell retention in the splenic marginal zone. *Science*. 2002;297(5580):409–412.
19. Pillai S, et al. Marginal zone B cells. *Annu Rev Immunol*. 2005;23:161–196.
20. Martin F, et al. Marginal zone and B1 B cells unite in the early response against T-independent blood-borne particulate antigens. *Immunity*. 2001;14(5):617–629.
21. Gunn KE, Brewer JW. Evidence that marginal zone B cells possess an enhanced secretory apparatus and exhibit superior secretory activity. *J Immunol*. 2006;177(6):3791–3798.
22. Gaudette BT, et al. mTORC1 coordinates an immediate unfolded protein response-related transcriptome in activated B cells preceding antibody secretion. *Nat Commun*. 2020;11(1):723.
23. Saito T, et al. Notch2 is preferentially expressed in mature B cells and indispensable for marginal zone B lineage development. *Immunity*. 2003;18(5):675–685.
24. Simonetti G, et al. IRF4 controls the positioning of mature B cells in the lymphoid microenvironments by regulating NOTCH2 expression and activity. *J Exp Med*. 2013;210(13):2887–2902.
25. Chan SM, et al. Notch signals positively regulate activity of the mTOR pathway in T-cell acute lymphoblastic leukemia. *Blood*. 2007;110(1):278–286.
26. Ciofani M, Zuniga-Pflucker JC. Notch promotes survival of pre-T cells at the beta-selection checkpoint by regulating cellular metabolism. *Nat Immunol*. 2005;6(9):881–888.
27. Sade H, et al. The anti-apoptotic effect of Notch-1 requires p56lck-dependent, Akt/PKB-mediated signaling in T cells. *J Biol Chem*. 2004;279(4):2937–2944.
28. Laplante M, Sabatini DM. mTOR signaling in growth control and disease. *Cell*. 2012;149(2):274–293.
29. Jones DD, et al. mTOR has distinct functions in generating versus sustaining humoral immunity. *J Clin Invest*. 2016;126(11):4250–4261.
30. Huang J, Manning BD. The TSC1-TSC2 complex: a molecular switchboard controlling cell growth. *Biochem J*. 2008;412(2):179–190.
31. Benhamron S, et al. mTOR activation promotes plasma cell differentiation and bypasses XBP-1 for immunoglobulin secretion. *Mol Cell Biol*. 2015;35(1):153–166.
32. Iwakoshi NN, et al. Plasma cell differentiation and the unfolded protein response intersect at the transcription factor XBP-1. *Nat Immunol*. 2003;4(4):321–329.
33. Weng AP, et al. c-Myc is an important direct target of Notch1 in T-cell acute lymphoblastic leukemia/lymphoma. *Genes Dev*. 2006;20(15):2096–2109.
34. Ryan RJH, et al. A B cell regulome links notch to downstream oncogenic pathways in small B cell lymphomas. *Cell Rep*. 2017;21(3):784–797.
35. Herranz D, et al. A NOTCH1-driven MYC enhancer promotes T cell development, transformation and acute lymphoblastic leukemia. *Nat Med*. 2014;20(10):1130–1137.
36. Topham C, et al. MYC is a major determinant of mitotic cell fate. *Cancer Cell*. 2015;28(1):129–140.
37. Kallies A, et al. Plasma cell ontogeny defined by quantitative changes in blimp-1 expression. *J Exp Med*. 2004;200(8):967–977.
38. Kreslavsky T, et al. β-Selection-induced proliferation is required for αβ T cell differentiation. *Immunity*. 2012;37(5):840–853.
39. Morice WG, et al. Rapamycin-induced inhibition of p34cdc2 kinase activation is associated with G1/S-phase growth arrest in T lymphocytes. *J Biol Chem*. 1993;268(5):3734–3738.
40. Diril MK, et al. Cyclin-dependent kinase 1 (Cdk1) is essential for cell division and suppression of DNA re-replication but not for liver regeneration. *Proc Natl Acad Sci U S A*. 2012;109(10):3826–3831.
41. Nygren JM, Bryder D. A novel assay to trace proliferation history in vivo reveals that enhanced division-

al kinetics accompany loss of hematopoietic stem cell self-renewal. *PLoS One*. 2008;3(11):e3710.
42. Wu Y, et al. Therapeutic antibody targeting of individual Notch receptors. *Nature*. 2010;464(7291):1052–1057.
43. Vembar SS, Brodsky JL. One step at a time: endoplasmic reticulum-associated degradation. *Nat Rev Mol Cell Biol*. 2008;9(12):944–957.
44. Fasnacht N, et al. Specific fibroblastic niches in secondary lymphoid organs orchestrate distinct Notch-regulated immune responses. *J Exp Med*. 2014;211(11):2265–2279.
45. de Alboran IM, et al. Analysis of C-MYC function in normal cells via conditional gene-targeted mutation. *Immunity*. 2001;14(1):45–55.
46. Heinzel S, et al. A Myc-dependent division timer complements a cell-death timer to regulate T cell and B cell responses. *Nat Immunol*. 2017;18(1):96–103.
47. Khalil AM, et al. B cell receptor signal transduction in the GC is short-circuited by high phosphatase activity. *Science*. 2012;336(6085):1178–1181.
48. Meena NK, et al. mTORC1 activation in B cells confers impairment of marginal zone microarchitecture by exaggerating cathepsin activity. *Immunology*. 2018;155(4):505–518.
49. Hozumi K, et al. Delta-like 1 is necessary for the generation of marginal zone B cells but not T cells in vivo. *Nat Immunol*. 2004;5(6):638–644.
50. Hampel F, et al. CD19-independent instruction of murine marginal zone B-cell development by constitutive Notch2 signaling. *Blood*. 2011;118(24):6321–6331.
51. Dammers PM, Kroese FG. Recruitment and selection of marginal zone B cells is independent of exogenous antigens. *Eur J Immunol*. 2005;35(7):2089–2099.
52. Martin F, Kearney JF. Positive selection from newly formed to marginal zone B cells depends on the rate of clonal production, CD19, and btk. *Immunity*. 2000;12(1):39–49.
53. Wen L, et al. Evidence of marginal-zone B cell-positive selection in spleen. *Immunity*. 2005;23(3):297–308.
54. Cancro MP, Kearney JF. B cell positive selection: road map to the primary repertoire? *J Immunol*. 2004;173(1):15–19.
55. Farmer JR, et al. Induction of metabolic quiescence defines the transitional to follicular B cell switch. *Sci Signal*. 2019;12(604):eaaw5573.
56. Zuccarino-Catania GV, et al. CD80 and PD-L2 define functionally distinct memory B cell subsets that are independent of antibody isotype. *Nat Immunol*. 2014;15(7):631–637.
57. Johnson JL, et al. The transcription factor T-bet Resolves memory B cell subsets with distinct tissue distributions and antibody specificities in mice and humans. *Immunity*. 2020;52(5):842–855.
58. Wei C, et al. A new population of cells lacking expression of CD27 represents a notable component of the B cell memory compartment in systemic lupus erythematosus. *J Immunol*. 2007;178(10):6624–6633.
59. Allie SR, et al. The establishment of resident memory B cells in the lung requires local antigen encounter. *Nat Immunol*. 2019;20(1):97–108.
60. Weill JC, et al. Human marginal zone B cells. *Annu Rev Immunol*. 2009;27:267–285.
61. Carsetti R, et al. Impairment of the antipolysaccharide response in splenectomized patients is due to the lack of immunoglobulin M memory B cells. *J Infect Dis*. 2006;193(8):1189–1190.
62. Descatoire M, et al. Identification of a human splenic marginal zone B cell precursor with NOTCH2-dependent differentiation properties. *J Exp Med*. 2014;211(5):987–1000.
63. Tumang JR, et al. Spontaneously Ig-secreting B-1 cells violate the accepted paradigm for expression of differentiation-associated transcription factors. *J Immunol*. 2005;174(6):3173–3177.
64. Fairfax KA, et al. Different kinetics of blimp-1 induction in B cell subsets revealed by reporter gene. *J Immunol*. 2007;178(7):4104–4111.
65. Kiel MJ, et al. Whole-genome sequencing identifies recurrent somatic NOTCH2 mutations in splenic marginal zone lymphoma. *J Exp Med*. 2012;209(9):1553–1565.
66. Rossi D, et al. The coding genome of splenic marginal zone lymphoma: activation of NOTCH2 and other pathways regulating marginal zone development. *J Exp Med*. 2012;209(9):1537–1551.
67. Chung J, et al. Fibroblastic niches prime T cell alloimmunity through Delta-like Notch ligands. *J Clin Invest*. 2017;127(4):1574–1588.
68. Calado DP, et al. The cell-cycle regulator c-Myc is essential for the formation and maintenance of germinal centers. *Nat Immunol*. 2012;13(11):1092–1100.
69. Kadauke S, Blobel GA. "Remembering" tissue-specific transcription patterns through mitosis. *Cell Cycle*. 2012;11(21):3911–3912.
70. Ma Y, et al. How the cell cycle impacts chromatin architecture and influences cell fate. *Front Genet*. 2015;6:19.
71. Kadauke S, et al. Tissue-specific mitotic bookmarking by hematopoietic transcription factor GATA1. *Cell*. 2012;150(4):725–737.
72. Chan WF, et al. Pre-mitotic genome re-organisation bookends the B cell differentiation process. *Nat Commun*. 2021;12(1):1344.
73. Chaffee BR, et al. Nuclear removal during terminal lens fiber cell differentiation requires CDK1 activity: appropriating mitosis-related nuclear disassembly. *Development*. 2014;141(17):3388–3398.
74. Kwiatkowski DJ, et al. A mouse model of TSC1 reveals sex-dependent lethality from liver hemangiomas, and up-regulation of p70S6 kinase activity in Tsc1 null cells. *Hum Mol Genet*. 2002;11(5):525–534.
75. Tran IT, et al. Blockade of individual Notch ligands and receptors controls graft-versus-host disease. *J Clin Invest*. 2013;123(4):1590–1604.
76. Wilmore JR, et al. Protocol for improved resolution of plasma cell subpopulations by flow cytometry. *Eur J Immunol*. 2017;47(8):1386–1388.
77. Bray NL, et al. Near-optimal probabilistic RNA-seq quantification. *Nat Biotechnol*. 2016;34(5):525–527.
78. Law CW, et al. voom: precision weights unlock linear model analysis tools for RNA-seq read counts. *Genome Biol*. 2014;15(2):R29.
79. Ritchie ME, et al. limma powers differential expression analyses for RNA-sequencing and microarray studies. *Nucleic Acids Res*. 2015;43(7):e47.
80. Huang da W, et al. Bioinformatics enrichment tools: paths toward the comprehensive functional analysis of large gene lists. *Nucleic Acids Res*. 2009;37(1):1–13.
81. Huang da W, et al. Systematic and integrative analysis of large gene lists using DAVID bioinformatics resources. *Nat Protoc*. 2009;4(1):44–57.
82. Bindea G, et al. ClueGO: a Cytoscape plug-in to decipher functionally grouped gene ontology and pathway annotation networks. *Bioinformatics*. 2009;25(8):1091–1093.
83. Mootha VK, et al. PGC-1alpha-responsive genes involved in oxidative phosphorylation are coordinately downregulated in human diabetes. *Nat Genet*. 2003;34(3):267–273.
84. Subramanian A, et al. Gene set enrichment analysis: a knowledge-based approach for interpreting genome-wide expression profiles. *Proc Natl Acad Sci U S A*. 2005;102(43):15545–15550.